Table 6. Pathologic characteristics and tracer uptake

	^{11}C-Choline				^{18}F-FDG			
	SUV_{max}	*P*-value	TBR	*P*-value	SUV_{max}	*P*-value	TBR	*P*-value
% Invasive component		0.979		0.432		0.934		0.79
>30%	3.7 ± 2.3		8.5 ± 5.6		4.4 ± 3.1		3.9 ± 2.4	
<30%	3.7 ± 3.5		7.4 ± 6.4		4.4 ± 3.1		4.1 ± 3.2	
Fibrocystic change		<0.0001		<0.0001		0.002		0.429
Present	5.4 ± 3.5		11.4 ± 6.7		5.7 ± 3.5		4.3 ± 2.2	
Absent	2.5 ± 1.6		5.7 ± 4.0		3.5 ± 2.5		3.8 ± 3.1	
Histologic grade		<0.0001		<0.0001		<0.0001		<0.0001
1 or 2	2.2 ± 1.1		4.4 ± 2.5		2.9 ± 2.0		2.9 ± 2.3	
3	5.3 ± 3.3		11.8 ± 6.2		6.1 ± 3.3		5.2 ± 2.8	
Nuclear grade		<0.0001		<0.0001		<0.0001		<0.0001
1 or 2	2.2 ± 1.1		4.4 ± 2.5		2.9 ± 2.0		2.9 ± 2.3	
3	5.3 ± 3.3		11.8 ± 6.2		6.1 ± 3.3		5.2 ± 2.8	
Structural grade		<0.0001		<0.0001		<0.0001		0.011
1 or 2	2.3 ± 1.5		4.7 ± 3.5		3.0 ± 2.4		3.1 ± 2.7	
3	4.8 ± 3.2		10.5 ± 6.3		5.5 ± 3.2		4.7 ± 2.7	
Nuclear atypia		<0.0001		<0.0001		<0.0001		0.012
1 or 2	2.1 ± 1.1		4.2 ± 2.4		2.8 ± 2.0		2.8 ± 2.3	
3	5.2 ± 3.3		11.6 ± 6.1		5.9 ± 3.2		5.1 ± 2.7	
Mitosis		<0.0001		<0.0001		<0.0001		<0.0001
1 or 2	2.1 ± 1.1		4.5 ± 2.5		2.8 ± 1.8		2.6 ± 2.1	
3	6.4 ± 3.0		13.8 ± 5.5		7.1 ± 3.0		6.3 ± 2.1	
Necrosis		0.046		0.001		0.051		0.529
Present	4.5 ± 3.2		10.6 ± 7.1		5.3 ± 3.3		4.2 ± 2.6	
Absent	3.1 ± 2.6		6.2 ± 4.3		3.8 ± 2.9		3.8 ± 2.9	
Fat invasion		0.003		0.002		0.024		0.061
Present	4.5 ± 3.3		9.6 ± 6.5		5.0 ± 3.4		4.4 ± 2.8	
Absent	2.4 ± 1.5		5.3 ± 3.6		3.4 ± 2.2		3.2 ± 2.6	
Cutaneous invasion		0.004		<0.0001		0.133		0.706
Present	6.4 ± 3.1		14.8 ± 7.3		6.0 ± 4.7		4.3 ± 2.2	
Absent	3.4 ± 2.7		7.2 ± 5.3		4.2 ± 2.8		3.9 ± 2.8	
HER-2/neu receptor		0.53		0.772		0.518		0.766
Positive	3.5 ± 2.6		8.2 ± 6.0		4.2 ± 2.7		4.1 ± 3.1	
Negative	3.9 ± 3.2		7.8 ± 6.0		4.7 ± 3.5		3.9 ± 2.5	
Estrogen receptor		<0.0001		<0.0001		<0.0001		<0.0001
Positive	2.3 ± 1.4		5.4 ± 3.4		3.1 ± 1.8		2.9 ± 2.9	
Negative	6.3 ± 3.3		13.1 ± 6.6		7.0 ± 3.5		6.1 ± 2.5	
Progesterone receptor		<0.0001		<0.0001		<0.0001		<0.0001
Positive	2.4 ± 1.5		5.6 ± 3.7		3.1 ± 1.9		2.9 ± 2.9	
Negative	6.2 ± 3.4		12.7 ± 6.8		7.0 ± 3.5		6.1 ± 2.5	
Triple negative		<0.001		<0.0001		<0.0001		0.002
Yes	6.7 ± 3.3		12.9 ± 6.5		7.4 ± 3.8		6.2 ± 2.1	
No	2.9 ± 2.2		6.7 ± 5.2		3.7 ± 2.4		3.4 ± 2.7	

FDG, fludeoxyglucose; SUV_{max}, maximum standardized uptake value; TBR, tumor-to-background ratio.

period is warranted to clarify the exact role of this technique and how it affects patient outcome.

Acknowledgments

This work was supported, in part, by a Grant-in-Aid for Cancer Research (21–5-2) from the Ministry of Health, Labour and Welfare of Japan.

Disclosure Statement

The authors declare that they have no conflicts of interest.

Abbreviations

CT	computed tomography
DCIS	ductal carcinoma *in situ*
ER	estrogen receptor
FCC	fibrocystic change
^{18}F-FDG2-[^{18}F]	fluoro-2-deoxy-D-glucose
HER-2/neu	human epidermal growth factor-2
MAPK	mitogen-activated protein kinase
SUV_{max}	maximum standardized uptake value
TBR	tumor-to-background ratio

References

1 Nieweg OE, Kim EE, Wong WH *et al.* Positron emission tomography with fluorine-18-deoxyglucose in the detection and staging of breast cancer. *Cancer* 1993; **71**: 3920–5.

2 Rosen EL, Eubank WB, Mankoff DA. FDG PET, PET/CT, and breast cancer imaging. *Radiographics* 2007; **27**: S215–29.

3 Mahner S, Schirrmacher S, Brenner W *et al.* Comparison between positron emission tomography using 2-[fluorine-18]fluoro-2-deoxy-D-glucose, conven-

doi: 10.1111/j.1349-7006.2012.02348.x

tional imaging and computed tomography for staging of breast cancer. *Ann Oncol* 2008; **19**: 1249–54.
4 Tatsumi M, Cohade C, Mourtzikos KA, Fishman EK, Wahl RL. Initial experience with FDG-PET/CT in the evaluation of breast cancer. *Eur J Nucl Med Mol Imaging* 2006; **33**: 254–62.
5 Lim HS, Yoon W, Chung TW *et al.* FDG PET/CT for the detection and evaluation of breast diseases: usefulness and limitations. *Radiographics* 2007; **27**: S197–213.
6 Pisano ED, Johnston RE, Chapman D *et al.* Human breast cancer specimens: diffraction-enhanced imaging with histologic correlation. Improved conspicuity of lesion detail compared with digital radiography. *Radiology* 2000; **214**: 895–901.
7 Venta LA, Wiley EL, Gabriel H, Adler YT. Imaging features of focal breast fibrosis: mammographic–pathologic correlation of noncalcified breast lesions. *AJR Am J Roentgenol* 1999; **173**: 309–16.
8 Chen JH, Liu H, Baek HM, Nalcioglu O, Su MY. Magnetic resonance imaging features of fibrocystic change of the breast. *Magn Reson Imaging* 2008; **26**: 1207–14.
9 van den Bosch MA, Daniel BL, Mariano MN *et al.* Magnetic resonance imaging characteristics of fibrocystic change of the breast. *Invest Radiol* 2005; **40**: 436–41.
10 Yutani K, Shiba E, Kusuoka H *et al.* Comparison of FDG-PET with MIBI-SPECT in the detection of breast cancer and axillary lymph node metastasis. *J Comput Assist Tomogr* 2000; **24**: 274–80.
11 Ishidate K. Choline/ethanolamine kinase from mammalian tissues. *Biochim Biophys Acta* 1997; **1348**: 70–8.
12 Uchida T, Yamashita S. Molecular cloning, characterization, and expression in *Escherichia coli* of a cDNA encoding mammalian choline kinase. *J Biol Chem* 1992; **267**: 10156–62.
13 Kenny LM, Contractor KB, Hinz R *et al.* Reproducibility of [^{11}C]choline-positron emission tomography and effect of trastuzumab. *Clin Cancer Res* 2010; **16**: 4236–45.
14 Fukukita H, Senda M, Terauchi T *et al.* Japanese guideline for the oncology FDG-PET/CT data acquisition protocol: synopsis of Version 1.0. *Ann Nucl Med* 2010; **24**: 325–34.
15 Hara T, Yuasa M. Automated synthesis of [^{11}C]choline, a positron-emitting tracer for tumor imaging. *Appl Radiat Isot* 1999; **50**: 531–3.
16 Sobin LH, Wittekind C. *UICC TNM Classification of Malignant Tumours*, 6th edn. New York: Wiley, 2002.
17 Elston CW, Ellis IO. Pathological prognostic factors in breast cancer. I. The value of histological grade in breast cancer: experience from a large study with long-term follow-up. *Histopathology* 2002; **41**: 154–61.
18 McCarty KS Jr, Szabo E, Flowers JL *et al.* Use of a monoclonal anti-estrogen receptor antibody in the immunohistochemical evaluation of human tumors. *Cancer Res* 1986; **46**: s4244–8.
19 Contractor KB, Kenny LM, Stebbing J *et al.* [^{11}C]choline positron emission tomography in estrogen receptor-positive breast cancer. *Clin Cancer Res* 2009; **15**: 5503–10.
20 Neubauer H, Li M, Kuehne-Held R, Schneider A, Kaiser WA. High grade and non-high grade ductal carcinoma *in situ* on dynamic MR mammography: characteristic findings for signal increase and morphological pattern of enhancement. *Br J Radiol* 2003; **76**: 3–12.
21 Guinebretière JM, Lê Monique G, Gavoille A, Bahi J, Contesso G. Angiogenesis and risk of breast cancer in women with fibrocystic disease. *J Natl Cancer Inst* 1994; **86**: 635–6.
22 Bodian CA, Perzin KH, Lattes R, Hoffmann P. Reproducibility and validity of pathologic classifications of benign breast disease and implications for clinical applications. *Cancer* 1993; **71**: 3908–13.
23 Revelon G, Sherman ME, Gatewood OM, Brem RF. Focal fibrosis of the breast: imaging characteristics and histopathologic correlation. *Radiology* 2000; **216**: 255–9.
24 Orel SG, Schnall MD, LiVolsi VA, Troupin RH. Suspicious breast lesions: MR imaging with radiologic–pathologic correlation. *Radiology* 1994; **190**: 485–93.
25 Fobben ES, Rubin CZ, Kalisher L, Dembner AG, Seltzer MH, Santoro EJ. Breast MR imaging with commercially available techniques: radiologic–pathologic correlation. *Radiology* 1995; **196**: 143–52.
26 Yutani K, Tatsumi M, Uehara T, Nishimura T. Effect of patients being prone during FDG PET for the diagnosis of breast cancer. *AJR Am J Roentgenol* 1999; **173**: 1337–9.
27 Palmedo H, Bender H, Grünwald F *et al.* Comparison of fluorine-18 fluorodeoxyglucose positron emission tomography and technetium-99*m* methoxyisobutylisonitrile scintimammography in the detection of breast tumours. *Eur J Nucl Med* 1997; **24**: 1138–45.
28 Kole AC, Nieweg OE, Pruim J *et al.* Standardized uptake value and quantification of metabolism for breast cancer imaging with FDG and l-[1–11C]tyrosine. *J Nucl Med* 1997; **38**: 692–6.
29 Yoshimoto M, Waki A, Obata A, Furukawa T, Yonekura Y, Fujibayashi Y. Radiolabeled choline as a proliferation marker: comparison with radiolabeled acetate. *Nucl Med Biol* 2004; **31**: 859–65.

Neoadjuvant Chemotherapy in Breast Cancer: Prediction of Pathologic Response with PET/CT and Dynamic Contrast-enhanced MR Imaging—Prospective Assessment [1]

Ukihide Tateishi, MD
Mototaka Miyake, MD
Tomoaki Nagaoka, PhD
Takashi Terauchi, MD
Kazunori Kubota, MD
Takayuki Kinoshita, MD
Hiromitsu Daisaki, PhD
Homer A. Macapinlac, MD

Purpose: To clarify whether fluorine 18 (^{18}F) fluorodeoxyglucose (FDG) positron emission tomography (PET)/computed tomography (CT) and dynamic contrast-enhanced (DCE) magnetic resonance (MR) imaging performed after two cycles of neoadjuvant chemotherapy (NAC) can be used to predict pathologic response in breast cancer.

Materials and Methods: Institutional human research committee approval and written informed consent were obtained. Accuracy after two cycles of NAC for predicting pathologic complete response (pCR) was examined in 142 women (mean age, 57 years; range, 43–72 years) with histologically proved breast cancer between December 2005 and February 2009. Quantitative PET/CT and DCE MR imaging were performed at baseline and after two cycles of NAC. Parameters of PET/CT and of blood flow and microvascular permeability at DCE MR were compared with pathologic response. Patients were also evaluated after NAC by using Response Evaluation Criteria in Solid Tumors (RECIST) 1.1 based on DCE MR measurements and European Organization for Research and Treatment of Cancer (EORTC) criteria and PET Response Criteria in Solid Tumors (PERCIST) 1.0 based on PET/CT measurements. Multiple logistic regression analyses were performed to examine continuous variables at PET/CT and DCE MR to predict pCR, and diagnostic accuracies were compared with the McNemar test.

Results: Significant decrease from baseline of all parameters at PET/CT and DCE MR was observed after NAC. Therapeutic response was obtained in 24 patients (17%) with pCR and 118 (83%) without pCR. Sensitivity, specificity, and accuracy to predict pCR were 45.5%, 85.5%, and 82.4%, respectively, with RECIST and 70.4%, 95.7%, and 90.8%, respectively, with EORTC and PERCIST. Multiple logistic regression revealed three significant independent predictors of pCR: percentage maximum standardized uptake value (%SUV_{max}) (odds ratio [OR], 1.22; 95% confidence interval [CI]: 1.11, 1.34; $P < .0001$), percentage rate constant (%κ_{ep}) (OR, 1.07; CI: 1.03, 1.12; $P = .002$), and percentage area under the time-intensity curve over 90 seconds (%AUC_{90}) (OR, 1.04; CI: 1.01, 1.07; $P = .048$). When diagnostic accuracies are compared, PET/CT is superior to DCE MR for the prediction of pCR (%SUV_{max} [90.1%] vs %κ_{ep} [83.8%] or %AUC_{90} [76.8%]; $P < .05$).

Conclusion: The sensitivities of %SUV_{max} (66.7%), %κ_{ep} (51.7%), and %AUC_{90} (50.0%) at ^{18}F-FDG PET/CT and DCE MR after two cycles of NAC are not acceptable, but the specificities (96.4%, 92.0%, and 95.2%, respectively) are high for stratification of pCR cases in breast cancer.

[1] From the Department of Radiology, Yokohama City University Graduate School of Medicine, 3-9 Fukuura, Kanazawa-ku, Yokohama, Kanagawa 236-0004, Japan (U.T.); Divisions of Diagnostic Radiology (M.M.) and Breast Surgery (T.K.), National Cancer Center Hospital, Tokyo, Japan; Electromagnetic Compatibility Group Applied Electromagnetic Research Center, National Institute of Information and Communications Technology, Tokyo, Japan (T.N.); Division of Cancer Screening, Research Center for Cancer Prevention and Screening, National Cancer Center, Tokyo, Japan (T.T., H.D.); Department of Radiology, Tokyo Medical Dental University Graduate School of Medicine, Tokyo, Japan (K.K.); and Division of Diagnostic Imaging, University of Texas MD Anderson Cancer Center, Houston, Tex (H.A.M.). Received June 7, 2011; revision requested July 13; revision received August 10; accepted September 1; final version accepted November 16. Supported in part by a Grant-in-Aid for Cancer Research (21-5-2) from the Ministry of Health, Labour and Welfare. **Address correspondence to** U.T. (e-mail: *utateish@yokohama-cu.ac.jp*).

Neoadjuvant chemotherapy (NAC) (see Table 1 for complete list of abbreviations) has been used as a primary therapeutic strategy in patients with breast cancer. For patients with locally advanced disease, the main therapeutic options to obtain potential cure are definitive NAC followed by surgery (1). A 5-year disease-specific survival of 96% has been reported in patients showing pathologic complete response (pCR) in response to induction NAC followed by resection (2). Previous studies have suggested that early response after NAC might be a predictor of pathologic response and could be associated with the long-term outcome (3,4).

Imaging of metabolic pathways serves as an alternative for visualizing the treatment effects; furthermore, metabolic reduction within the tumor precedes the anatomic responses to therapy. Positron emission tomography (PET) with fluorine 18 (^{18}F) fluorodeoxyglucose (FDG) has been used to evaluate the clinical response to NAC in patients with breast cancer (5,6). Metabolic reduction often occurs early in the course of therapy and precedes reduction in the size of the tumor, because morphologic changes in the tumor occur much later than the metabolic response. The ^{18}F-FDG uptake, expressed semiquantitatively by the standardized uptake value (SUV), in interim PET studies has been reported as a strong predictor of clinical or pathologic response (7–10). Metabolic reduction detected between baseline and the early phase of NAC can provide early information on the potential tumor response (11,12).

Quantification of blood flow within a tumor by using dynamic contrast-enhanced (DCE) magnetic resonance (MR) imaging has also been reported to provide accurate information while monitoring the effects of chemotherapy in patients with breast cancer. DCE MR imaging allows measurements of the kinetic parameters related to perfusion and permeability. Pharmacodynamic markers obtained by means of sequential DCE MR imaging are sensitive for early detection of the response to chemotherapy in breast cancer and can be predictive of a pathologic response after chemotherapy (13–15). In addition, DCE MR imaging parameters, including the transfer constant (K^{trans}), rate constant (κ_{ep}), and area under the curve are reported as potent predictors of the treatment outcome (16,17).

Although data from both sequential PET and DCE MR imaging allow more precise visualization of the tumor response to NAC, the relationship between the data from sequential PET and those from DCE MR imaging for assessment of the tumor response to NAC in breast cancer has not yet been fully elucidated. Mankoff et al (18,19) reported the existence of an association between glucose metabolism and blood flow by using ^{18}F-FDG and oxygen 15 (^{15}O)-water PET in patients with locally advanced breast cancer receiving NAC, because hypoxia-induced angiogenesis results in increased glycolysis and expression of glycolytic enzymes. We consider that ^{18}F-FDG PET/computed tomographic (CT) images reflect the changes in metabolism within tumors, which are not always related to the blood flow and microvascular permeability evaluated at DCE MR imaging. The purpose of our study was to clarify whether ^{18}F-FDG PET/CT and DCE MR imaging performed after two cycles of NAC can be used to predict pathologic response in patients with breast cancer.

Advances in Knowledge

- The sensitivity of percentage maximum standardized uptake value (%SUV_{max}) (66.7%), percentage rate constant (%κ_{ep}) (51.7%), and percentage area under the time-intensity curve until 90 seconds (%AUC_{90}) (50.0%) obtained with fluorine 18–fluorodeoxyglucose (FDG) PET/CT and dynamic contrast-enhanced (DCE) MR imaging after two cycles of neoadjuvant chemotherapy are not acceptable, but the specificity of %SUV_{max} (96.4%), %κ_{ep} (92.0%), and %AUC_{90} (95.2%) are high for stratification of pathologic complete response (pCR) cases in breast cancer.
- Multiple logistic regression revealed three significant independent predictors of pCR: %SUV_{max} (odds ratio, 1.22; 95% confidence interval [CI], 1.11, 1.34; $P < .0001$), %κ_{ep} (odds ratio, 1.07; 95% CI: 1.03, 1.12; $P = .002$), and %AUC_{90} (odds ratio, 1.04; 95% CI: 1.01, 1.07; $P = .048$).
- When diagnostic accuracies of the two modalities are compared, FDG PET/CT is superior to DCE MR imaging in the prediction of pCR (%SUV_{max} [90.1%] vs %κ_{ep} [83.8%] or %AUC_{90} [76.8%]; $P < .05$).

Implication for Patient Care

- FDG PET/CT is more accurate than DCE MR imaging as an interim modality to predict pCR.

Materials and Methods

Patient Eligibility

This study was conducted with the approval of the local ethics committee at four institutions (two cancer institutions and two academic hospitals) after obtaining written informed consent

Published online
10.1148/radiol.12111177 **Content code:** BR

Radiology 2012; 263:53–63

Author contributions:
Guarantors of integrity of entire study, U.T., T.T.; study concepts/study design or data acquisition or data analysis/interpretation, all authors; manuscript drafting or manuscript revision for important intellectual content, all authors; approval of final version of submitted manuscript, all authors; literature research, U.T.; clinical studies, U.T., M.M., T.T., T.K.; experimental studies, T.N., H.D.; statistical analysis, U.T.; and manuscript editing, U.T., K.K., T.K., H.A.M.

Potential conflicts of interest are listed at the end of this article.

Table 1

List of Abbreviations

Abbreviation	Definition
AUC_{90}	Area under the time-intensity curve until 90 seconds
CI	Confidence interval
DCE	Dynamic contrast enhanced
EORTC	European Organization for Research and Treatment of Cancer
FDG	Fluorodeoxyglucose
κ_{ep}	Rate constant
K^{trans}	Transfer constant
NAC	Neoadjuvant chemotherapy
pCR	Pathologic complete response
PERCIST	PET Response Criteria in Solid Tumors
RECIST	Response Evaluation Criteria in Solid Tumors
ROI	Region of interest
SUL	SUV corrected for lean body mass
$SUL_{50\%}$	Mean SUL at 50% of SUL_{peak}
SUL_{peak}	Peak SUL
$SUL_{70\%}$	Mean SUL at 70% of SUL_{peak}
SUV	Standardized uptake value
SUV_{max}	Maximum SUV
TLG	Total lesion glycolysis

from each of the patients. Patients with breast cancer that was proved histologically between December 2005 and February 2009 were enrolled. All patients underwent initial staging based on a review of the medical history, physical examinations, and imaging studies, including DCE MR imaging and PET/CT. The criteria for eligibility were as follows: histologically proved breast cancer without any history of treatment prior to the study, patient age between 20 and 70 years, and adequate organ function. The exclusion criteria were poor physical condition (inability to perform all predisease activities without restriction [n = 5] or inability to carry out work of a light or sedentary nature [n = 3]), tumor with skin involvement (n = 3), tumor with inflammatory change (n = 3), uncontrolled diabetes (n = 2), pregnancy (n = 1), apparent infection (n = 1), other serious medical disorder (n = 1), or concomitant malignancy (n = 1). A total of 20 patients were excluded from our study.

Neoadjuvant Chemotherapy

Patients received either *(a)* four cycles of 5-fluorouracil (500 mg/m^2), epirubicin (100 mg/m^2), and cyclophosphamide (500 mg/m^2) plus 12 cycles of weekly paclitaxel (80 mg/m^2), *(b)* four cycles of adriamycin (60 mg/m^2) and cyclophosphamide (500 mg/m^2) plus 12 cycles of weekly paclitaxel (80 mg/m^2), or *(c)* four cycles of 5-fluorouracil (500 mg/m^2), epirubicin (100 mg/m^2), and cyclophosphamide (500 mg/m^2) plus 12 cycles of weekly docetaxel (75 mg/m^2). Patients with HER-2 receptor–positive disease additionally received weekly herceptin (initial dose, 4 mg per kilogram of body weight; subsequent dose, 2 mg/kg). After completion of NAC, all patients underwent surgical resection.

DCE MR Imaging

DCE MR imaging was performed at baseline, within a week prior to the start of NAC, and at the end of cycle 2. All DCE MR images were acquired with a 3-T whole-body magnet system equipped with a dedicated receive-only four-channel dual breast coil (Magnetom Trio, A Tim System; Siemens Medical Systems, Erlangen, Germany). A transverse fat-saturated T2-weighted gradient-recalled echo examination was performed with a 25–35-cm field of view set to encompass both breasts and the axilla (repetition time msec/echo time msec, 4000/76.0; 170° flip angle; section thickness, 3 mm; and matrix, 288 × 384 pixels). DCE MR images were obtained with a three-dimensional spoiled gradient-echo snapshot flash sequence in the sagittal plane (3.74/1.38, 12° flip angle, section thickness of 0.8 mm, and matrix of 192–256 × 192–256 pixels). Low-molecular-weight gadolinium chelate, 0.1 mmol/kg (Magnevist; Bayer-Schering, Berlin, Germany), was injected intravenously at 3.0 mL/sec followed by a 20-mL normal saline flush by an automatic injector (Sonicshot GX; Nemoto Kyorindo, Kyoto, Japan). Continuous 10-second data acquisition was performed before, during, and after administration of contrast medium for a total of 4 minutes with 24 repeated data sets.

The quantitative parameters were measured for a region of interest (ROI) defined manually by a reader, separately in the tumor and aorta. The profile of the tumor was constant throughout the image sequence resulting in encompassing of over 95% of the tumor area. Errors related to ROI placement were minimized by evaluating the anatomic images and recording the sites of the ROIs. We applied a two-compartment pharmacokinetic model to the time-course of MR imaging enhancement. Dynamic gadolinium concentration curves were generated by using the signal enhancement ratio and the baseline tumor T1 relaxation time. Time-courses of gadolinium transfer into the tumor interstitium were subjected to nonlinear least squares fitting according to a two-compartment pharmacokinetic model (20). The following equation relating tumor gadolinium concentration, Ct(t), to arterial plasma gadolinium concentration, Cp(t), was used for the analyses: $dC(t)/dt = K^{trans}\,Cp(t) - \kappa_{ep}\cdot C(t)$, where K^{trans} and κ_{ep} were measured in 1/min. The area under the curve (in mmol/L·sec) was calculated as the area under the time-intensity curve until 90 seconds (AUC_{90}) after arrival of the bolus. The pharmacokinetic parameters of DCE MR imaging and the curve fitting were performed by using in-house software and were conducted by two of the authors (T.N., an MR technologist

with 10 years of experience; U.T., a radiologist with oncologic and nuclear medicine expertise with 16 years of experience).

PET/CT

A phantom study of PET/CT was performed to ensure quality control prior to the clinical study at all institutions (21). Studies were performed with a whole-body PET/CT scanner (Biograph 16, Siemens Medical Systems, or Aquiduo PCA-7000B, Toshiba, Otawara, Japan). The CT component of the scanner has a 16-row detector. We used a NEMA image quality phantom (NU 2–2001) for cross calibration. The radioactivity concentration of the background was set at 2.6 kBq/mL ± 0.2 (standard deviation) of ^{18}F-FDG, similar to that in the clinical condition. The radioactivity concentration of the hot portion was four times greater than that of the background. Data collection was performed for 2–5 minutes in dynamic acquisition and 30 minutes in static acquisition. Acquired data, including the normalization data, cross-calibration data, blank scan data, and transmission data were assessed for visual inspection, phantom noise equivalent count ($NEC_{phantom}$), percentage contrast ($Q_{H,\ 10mm}$), and percentage background variability (N_{10mm}). The preferred parameters pertinent to the clinical condition were $NEC_{phantom}$ greater than 10.4 (counts), N_{10mm} less than 6.2%, and $Q_{H,\ 10mm}/N_{10mm}$ greater than 1.9%. After a review of the data analyses, the optimum conditions for the scan were determined for PET/CT with the Biograph 16 scanner: data acquisition, 120 seconds per bed; field of view, 500 mm; iteration, 3; subset, 8; matrix size, 128 × 128; filter, Gaussian 5 mm in full width at half maximum; reconstruction, attenuation-weighted ordered-subsets expectation maximization (n = 20 [21%]). The optimum conditions for PET/CT were also determined with the Aquiduo PCA-7000B scanner: data acquisition, 180 seconds for one bed; field of view, 500 mm; iteration, 4; subset, 14; matrix size, 128 × 128; filter, Gaussian 8 mm in full width at half maximum; reconstruction, attenuation-weighted ordered-subsets expectation maximization (n = 122 [79%]). Patients received an intravenous injection of 3.7 MBq/kg of ^{18}F-FDG after at least 6 hours of fasting, followed by an uptake phase at 63 minutes ± 3. The patients were then placed in a supine, arm-up position, immediately after they had evacuated their bladders. For PET/CT, low-dose CT data were first acquired at 120-kVp by using an auto exposure control system, beam pitch of 0.875 or 1, and 1.5- or 2-mm × 16-row mode. Data acquisition was performed for each patient from the top of the skull to the midthigh. All PET/CT studies were performed at baseline and after two cycles of NAC.

Image Interpretation

The PET and CT images in all standard planes were reviewed on the e-soft workstation (Siemens Medical Systems, Iselin, NJ) or the Vox-base SP1000 workstation (J-MAC systems, Sapporo, Japan). Images were analyzed in consensus by two nuclear medicine physicians (T.T., with 26 years of experience, and U.T.). For the qualitative analysis, abnormal ^{18}F-FDG uptake was defined as activity substantially greater than that in the aortic blood on the attenuation-corrected images. Only the lesion that exhibited the most substantial uptake was selected as the target lesion to determine the response to therapy. An ROI was outlined within areas of increased ^{18}F-FDG uptake and measured on each section. When the lesion was heterogeneous, the ROI was set so as to cover all of the components of the lesion. Qualitative evaluation for focally increased glucose metabolism, as well as quantitative evaluation of the SUV was performed. The SUV was calculated according to the following equation: SUV = maximal count × calibration factor (in kilobecquerels per milliliter)/injected activity (in megabecquerels)/body weight (in kilograms). SUV corrected for lean body mass (SUL) was also calculated by maximal 1.2-cm diameter ROI set in tumor (22). Maximum values were used to minimize the partial volume effects and to increase the reproducibility of the measurements (23). Uptake measurements were made for maximum tumor-voxel SUL. $SUL_{50\%}$ and $SUL_{70\%}$ were mean SUL at 50% and 70% of peak SUL (SUL_{peak}) as exploratory data. The maximum SUV (SUV_{max}), SUL_{peak}, $SUL_{50\%}$, and $SUL_{70\%}$ measured on every scan were used as continuous variables.

Response Evaluation

The longest diameter was measured at baseline and after completion of NAC. Evaluation of the metabolic response was accomplished by comparing the relative changes in the SUV or SUL (%SUV or %SUL). The SUV or SUL on the PET/CT images obtained after completion of two cycles of NAC was compared with those obtained from the baseline study. Total lesion glycolysis (TLG) and the percent change in TLG (%TLG) were calculated as the response score (16) based on the volume (Vol) obtained at PET and the average SUV (SUV_{ave}) by using the formula: $\%TLG = \{[(SUV_{ave})_{pre} \times Vol_{pre} - (SUV_{ave})_{post} \times Vol_{post})]/(SUV_{ave})_{pre} \times Vol_{pre}\} \times 100$, where pre and post indicate measurements at baseline and after the completion of NAC.

Patients were also evaluated for response after two cycles of NAC by using the Response Evaluation Criteria in Solid Tumors (RECIST) 1.1 based on measurements of DCE MR imaging as well as European Organization for Research and Treatment of Cancer (EORTC) criteria and the PET Response Criteria in Solid Tumors (PERCIST) 1.0 based on measurements of ^{18}F-FDG PET/CT (22,24,25). Categories of RECIST 1.1 were complete response, partial response, stable disease, and progressive disease. For the EORTC criteria, complete metabolic response is defined as complete resolution of ^{18}F-FDG uptake within the tumor, so that it is indistinguishable from that of the surrounding normal tissue (22). Partial metabolic response was defined as greater than 25% reduction of the tumor SUV_{max} after the completion of NAC. Stable metabolic disease was defined as an increase in the tumor SUV_{max} by less than 25% or a decrease of the value by less than 15%, and no visible increase in the extent of tumor uptake (20% in longest diameter). Progressive metabolic disease was defined as an increase of the SUV_{max} by greater than 25% within the tumor region defined on the baseline scan, visible increase in the

extent of tumor uptake, or appearance of new uptake in metastatic lesions. In the recently proposed PERCIST 1.0 criteria, the target lesion should be evaluated by the SUL in a maximum of a 12-mm diameter volume ROI in the tumor (23). Complete metabolic response was defined as complete resolution of the ^{18}F-FDG uptake so that it was less than the mean liver activity and indistinguishable from the surrounding background blood-pool levels. Partial metabolic response was defined as reduction of the minimum of the 30% SUL_{peak} or absolute drop in the SUL by at least 0.8 SUL units. Progressive metabolic disease was defined as an increase by greater than 30% of the SUL_{peak} with an increase by 0.8 unit of the SUL_{peak} from that in the baseline scan and in a pattern not consistent with infection or treatment effect, visible increase in the extent of tumor uptake (75% in TLG, with no decline in the SUL), or appearance of new avid lesions. Stable metabolic disease was defined as not complete metabolic response, partial metabolic response, or progressive metabolic disease.

Table 2

Demographic and Clinical Data at Presentation in Patients with Breast Cancer

Parameter	Finding
Mean age (y)*	57 ± 6 (43–72)
Predominant area of tumor	
Medial upper quadrant	57 (40)
Lateral upper quadrant	51 (36)
Medial lower quadrant	20 (14)
Central (areola and nipple)	9 (6)
Lateral lower quadrant	5 (4)
Pathologic nodal status	
n1	122 (86)
n2	15 (11)
n3	5 (4)
Pathologic stage	
I	9 (6)
IIA	26 (18)
IIB	69 (49)
IIIA	19 (13)
IIIB	4 (3)
IIIC	15 (11)
Regimen of NAC	
FEC and paclitaxel	105 (74)
FEC, paclitaxel, and herceptin	5 (4)
FEC and docetaxel	4 (3)
AC and paclitaxel	28 (20)
Surgery	
Mastectomy and lymph node dissection†	88 (62)
Wide local resection and lymph node dissection	39 (27)
Quadrantectomy and lymph node dissection	15 (11)
Receptor positivity	
Estrogen receptor	100 (70)
Progesterone receptor	82 (58)
HER-2/neu	111 (78)
Final diagnosis	
Invasive ductal carcinoma	131 (92)
Invasive lobar carcinoma	11 (8)

Note.— Except where indicated, data are numbers of patients, and the numbers in parentheses are percentages. Lymph node dissection indicates sentinel and axillary lymph node dissection. AC = adriamycin and cyclophosphamide, FEC = 5-fluorouracil, epirubicin, and cyclophosphamide.

* Data are mean ± standard deviation, with the range in parentheses.

† Sampling of parasternal and subclavian lymph nodes was also performed.

Reference Standard

Core-needle biopsies of the primary tumor were performed before the initiation of treatment, and additional tumor tissue was obtained at the time of definitive surgery. Pathologic response to NAC (pCR or non-pCR) was evaluated by one of two pathologists (each with 20 years of experience) (26). Two radiologists (M.M., with 8 years of experience, and T.T.) conducted a retrospective review of the medical records and the follow-up radiographic assessments, which was performed after completion of NAC in consensus to ensure that findings from the research study were similar to those in the clinical interpretations. No difference was found from the clinical interpretations.

Statistical Analysis

Comparison of the means between groups was performed by using a three-way analysis of variance with Bonferroni adjustment for multiple comparisons. Multiple logistic regression analyses were performed to test the independence of established factors for the prediction of pCR. Multiple logistic regression analysis was performed by using all of the following continuous covariates: percent change in longest diameter, $\%SUV_{max}$, %TLG, posttreatment K^{trans}, $\%K^{trans}$, posttreatment κ_{ep}, $\%\kappa_{ep}$, posttreatment AUC_{90}, and $\%AUC_{90}$. Additional analysis was performed by using combined $\%SUV_{max}$ and $\%\kappa_{ep}$ and combined $\%SUV_{max}$ and $\%AUC_{90}$. Although $\%SUL_{peak}$, $\%SUL_{50\%}$, and $\%SUL_{70\%}$ have a discriminative power between patients with pCR and those without pCR, these values are not independent to $\%SUV_{max}$ and are excluded from covariates. Continuous variables determined by means of PET/CT and DCE MR imaging were included in the initial multivariate model. Receiver operating characteristic curves for the prediction of pCR were generated to determine the cutoff value that yielded optimal sensitivity and specificity. The

differences in sensitivity, specificity, positive predictive value, negative predictive value, and accuracy were compared by using the McNemar test. The *P* values calculated were two-sided, and $P < .05$ was considered to be indicative of statistical significance. Bonferroni adjustment was performed for the number of multiple comparisons in three-way analysis of variance and its *P* values of less than .016 were considered to indicate significance. Statistical analysis was performed with the PASW Statistics 19 software program (IBM, Tokyo, Japan).

Results

The analyses were based on the data obtained from a total of 142 women (Table 2). Stage IIB breast tumors were the most common (49%), followed by stage IIA (18%) and stage IIIA (13%) breast tumors. In all, 19% of the tumors were less than 2 cm in diameter, 73% were in the 2–5-cm range, and 8% were larger than 5 cm in diameter. Invasive ductal carcinoma (92%) was the most common histologic subtype, followed by invasive lobar carcinoma (8%). A statistically significant difference was found in SUV_{max} at baseline between invasive ductal carcinoma and invasive lobar carcinoma (7.9 ± 3.8 vs 5.0 ± 1.8, $P = .013$). Therapeutic response revealed pCR in 24 patients (17%) and non-pCR in the remaining 118 patients (83%) after completion of the NAC. The mean interval between baseline and final assessment was 30 months (range, 24–62 months).

All tumors showed substantial enhancement on DCE MR images. After two cycles of the NAC, a reduction of longest diameter from the baseline was observed in pCR cases (Table 3). The percent change in longest diameter did not differ between patients with and those without pCR (Table 4). After two cycles of NAC, decrease in the K^{trans}, κ_{ep}, and AUC_{90} from baseline was observed (Figs 1–3). Although the baseline K^{trans} values were similar between the two groups, the K^{trans} after two cycles of NAC was marginal in patients with pCR and those without pCR (0.11 ± 0.21 vs 0.38 ± 0.47; $P = .048$). Baseline AUC_{90} in patients with pCR was higher than in those without pCR (5.09 ± 1.84 vs 3.84 ± 1.30) but this value was lower after two cycles of NAC (1.50 ± 3.00 vs 2.48 ± 1.78; $P < .0001$). The κ_{ep} values in patients with pCR were higher than in those without pCR at baseline (3.60 ± 1.02 vs 2.77 ± 1.42) and were lower after two cycles of NAC (0.46 ± 0.92 vs 1.40 ± 1.01, $P < .0001$). The difference in $\%AUC_{90}$ between patients with and those without pCR was significant (73.4 ± 10.8 vs 33.9 ± 4.6; $P = .001$). No significant difference in the $\%K^{trans}$ or $\%\kappa_{ep}$ was found between the two groups (Table 4).

Decrease of the SUV_{max}, SUL_{peak}, $SUL_{50\%}$, $SUL_{70\%}$, and TLG from baseline was also observed after two cycles of NAC (Table 3, Fig 1). These values changed in a similar fashion to the $\%K^{trans}$, $\%\kappa_{ep}$, and $\%AUC_{90}$ during the course of NAC, especially in patients showing pCR. There were significant differences between the pCR and non-pCR groups in the SUV_{max} (0.9 ± 0.2 vs 2.7 ± 3.5, $P = .001$), SUL_{peak} (0.5 ± 0.1 vs 1.5 ± 1.9, $P = .006$), $SUL_{50\%}$ (0.4 ± 0.1 vs 1.1 ± 1.2, $P = .013$), and $SUL_{70\%}$ (0.4 ± 0.2 vs 1.3 ± 1.6, $P = .013$) after two cycles of NAC. Patients with pCR had higher $\%SUV_{max}$, $\%SUL_{peak}$, $\%SUL_{50\%}$, and $\%SUL_{70\%}$ values than those without pCR ($P = .001$); however, the %TLG did not differ significantly between the two groups (Table 4).

Table 3

PET/CT and DCE MR Imaging Parameters at Baseline and after Two Cycles of NAC

Parameter	Baseline	After NAC
Diameter (mm)	31.6 ± 13.2	23.6 ± 16.5
K^{trans} (1/min)	1.3 ± 1.2	0.3 ± 0.4
κ_{ep} (1/min)	2.9 ± 1.4	1.2 ± 1.1
AUC_{90} (mmol/L·sec)	40.7 ± 13.7	23.1 ± 21.2
SUV_{max} (g/mL)	7.7 ± 3.5	2.4 ± 1.6
SUL_{peak} (g/mL)	4.3 ± 2.1	1.3 ± 1.8
$SUL_{50\%}$ (g/mL)	3.2 ± 1.6	1.0 ± 1.2
$SUL_{70\%}$ (g/mL)	3.9 ± 1.9	1.2 ± 1.5
TLG ($g \cdot 10^{-3}$)	78.9 ± 106.5	24.1 ± 40.4
Liver SUL (g/mL)	1.6 ± 0.1	1.5 ± 0.4
Liver standard deviation (g/mL)	0.12 ± 0.03	0.11 ± 0.03

Note.—Data are mean ± standard deviation.

Table 4

Percent Changes in Parameters after Two Cycles of NAC

Parameter	pCR Group	Non-pCR Group	*P* Value
No. of patients*	24 (17)	118 (83)	
%Diameter	36.8 ± 40.2	−6.4 ± 181.5	.250
$\%K^{trans}$	53.0 ± 27.4	49.3 ± 52.8	.752
$\%\kappa_{ep}$	53.5 ± 16.2	32.3 ± 52.2	.052
$\%AUC_{90}$	73.4 ± 10.8	33.9 ± 4.6	.001
$\%SUV_{max}$	89.0 ± 2.9	62.5 ± 31.8	<.0001
$\%SUL_{peak}$	88.8 ± 4.8	62.5 ± 32.2	<.0001
$\%SUL_{50\%}$	88.4 ± 5.0	62.8 ± 30.6	<.0001
$\%SUL_{70\%}$	88.9 ± 5.0	63.4 ± 31.8	<.0001
%TLG	76.2 ± 20.6	50.6 ± 55.0	.078

Note.—Except where indicated, data are mean ± standard deviation of the percent change in the given parameter.

* Numbers in parentheses are percentages.

Figure 1

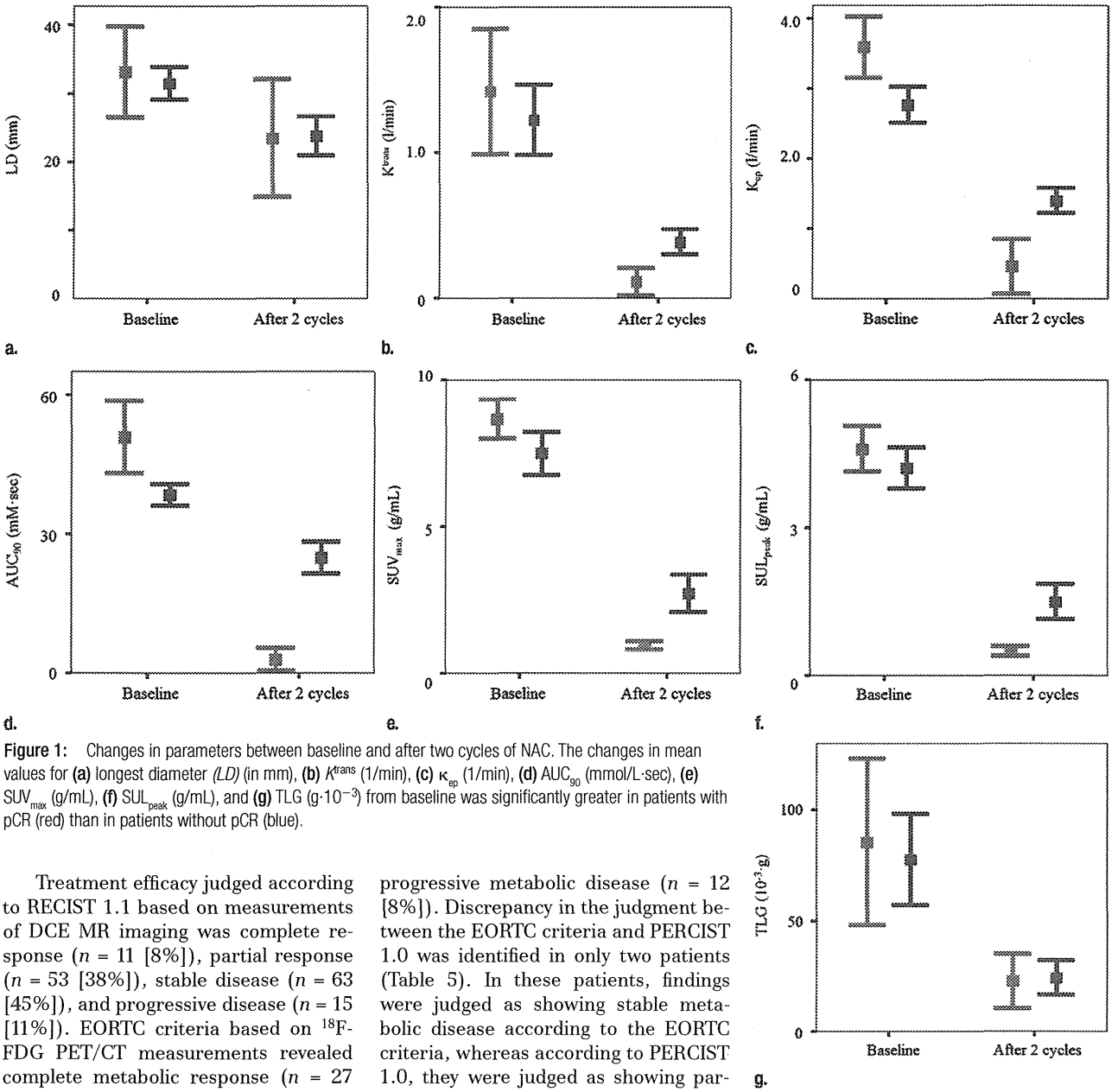

Figure 1: Changes in parameters between baseline and after two cycles of NAC. The changes in mean values for **(a)** longest diameter *(LD)* (in mm), **(b)** K^{trans} (1/min), **(c)** κ_{ep} (1/min), **(d)** AUC_{90} (mmol/L·sec), **(e)** SUV_{max} (g/mL), **(f)** SUL_{peak} (g/mL), and **(g)** TLG ($g \cdot 10^{-3}$) from baseline was significantly greater in patients with pCR (red) than in patients without pCR (blue).

Treatment efficacy judged according to RECIST 1.1 based on measurements of DCE MR imaging was complete response (n = 11 [8%]), partial response (n = 53 [38%]), stable disease (n = 63 [45%]), and progressive disease (n = 15 [11%]). EORTC criteria based on ^{18}F-FDG PET/CT measurements revealed complete metabolic response (n = 27 [19%]), partial metabolic response (n = 99 [70%]), stable metabolic disease (n = 4 [3%]), and progressive metabolic disease (n = 12 [8%]). Judgment of the treatment efficacy according to PERCIST 1.0 based on ^{18}F-FDG PET/CT measurements was complete metabolic response (n = 27 [19%]), partial metabolic response (n = 97 [69%]), stable metabolic disease (n = 6 [4%]), and progressive metabolic disease (n = 12 [8%]). Discrepancy in the judgment between the EORTC criteria and PERCIST 1.0 was identified in only two patients (Table 5). In these patients, findings were judged as showing stable metabolic disease according to the EORTC criteria, whereas according to PERCIST 1.0, they were judged as showing partial metabolic response, because these two patients had $\%SUV_{max}$ of 10% and 13% and $\%SUL_{peak}$ of 32% and 30%. The sensitivity, specificity, positive predictive value, negative predictive value, and accuracy of RECIST 1.1 for pCR were 45.5% (95% confidence interval [CI]: 37.4%, 53.6%), 85.5% (95% CI: 79.8%, 91.2%), 20.8% (95% CI: 14.1%, 27.5%), 94.9% (95% CI: 91.3%, 98.5%), and 82.4% (95% CI: 76.1%, 88.7%), respectively. Similar results for the diagnostic accuracy were obtained between the EORTC criteria and PERCIST 1.0, with a sensitivity, specificity, positive predictive value, negative predictive value, and accuracy for pCR of 70.4% (95% CI: 62.9%, 77.9%), 95.7% (95% CI: 92.4%, 99.0%), 79.2% (95%

CI: 72.5%, 85.9%), 93.2% (95% CI: 89.0%, 97.4%), and 90.8% (95% CI: 86.0%, 95.6%), respectively. Significant differences were found in sensitivity ($P < .05$), specificity ($P < .05$), and positive predictive value ($P < .05$) between RECIST 1.1 and EORTC criteria or PERCIST 1.0.

The significant predictive value of the factors identified in this population for pCR, including the $\%SUV_{max}$, $\%\kappa_{ep}$, and $\%AUC_{90}$, approached statistical significance (Table 6). The predictive value of the percent change in longest diameter, %TLG, posttreatment K^{trans}, $\%K^{trans}$, posttreatment κ_{ep}, and posttreatment AUC_{90} did not reach statistical significance. When combined $\%SUV_{max}$ and $\%\kappa_{ep}$ and combined $\%SUV_{max}$ and $\%AUC_{90}$ were adapted as covariates, the odds ratio of combined $\%SUV_{max}$ and $\%\kappa_{ep}$ showed statistical significance (1.10; 95% CI: 1.03, 1.36; $P = .031$). However, the odds ratio calculated with combined $\%SUV_{max}$ and $\%\kappa_{ep}$ was smaller compared with those of $\%SUV_{max}$ (Table 6). When a cutoff value derived from the receiver operating characteristic curve was adapted, the sensitivity, specificity, positive predictive value, negative predictive value, and accuracy of $\%SUV_{max}$, $\%\kappa_{ep}$, and $\%AUC_{90}$ for pCR were presented in Table 7. Significant difference was found in sensitivity ($P < .05$), positive predictive value ($P < .05$), negative predictive value ($P < .05$), and accuracy ($P < .05$) between $\%SUV_{max}$ and $\%\kappa_{ep}$ or $\%AUC_{90}$. This result suggests that $\%SUV_{max}$ is superior to $\%\kappa_{ep}$ or $\%AUC_{90}$ to predict pCR.

Discussion

Our data show that evaluation of response according to metabolism at PET/CT and blood flow and microvascular permeability at DCE MR imaging allow prediction of the pathologic response to NAC in patients with breast cancer. The results of multiple logistic regression analysis identified the $\%SUV_{max}$, $\%\kappa_{ep}$, and $\%AUC_{90}$ as independent predictors of pCR. Despite the ability of PET/CT alone (5–9) or DCE MR imaging alone (13–15) to be used to predict the response to NAC in patients with breast cancer, this is the first demonstration, to the best of our knowledge, of the discriminatory power of the $\%SUV_{max}$, $\%\kappa_{ep}$, and $\%AUC_{90}$ in predicting pCR after NAC compared with the direct predictive value of the parameters obtained from DCE MR imaging.

Multiple studies have also demonstrated the possibility of predicting the response to NAC with high accuracy by

Figure 2

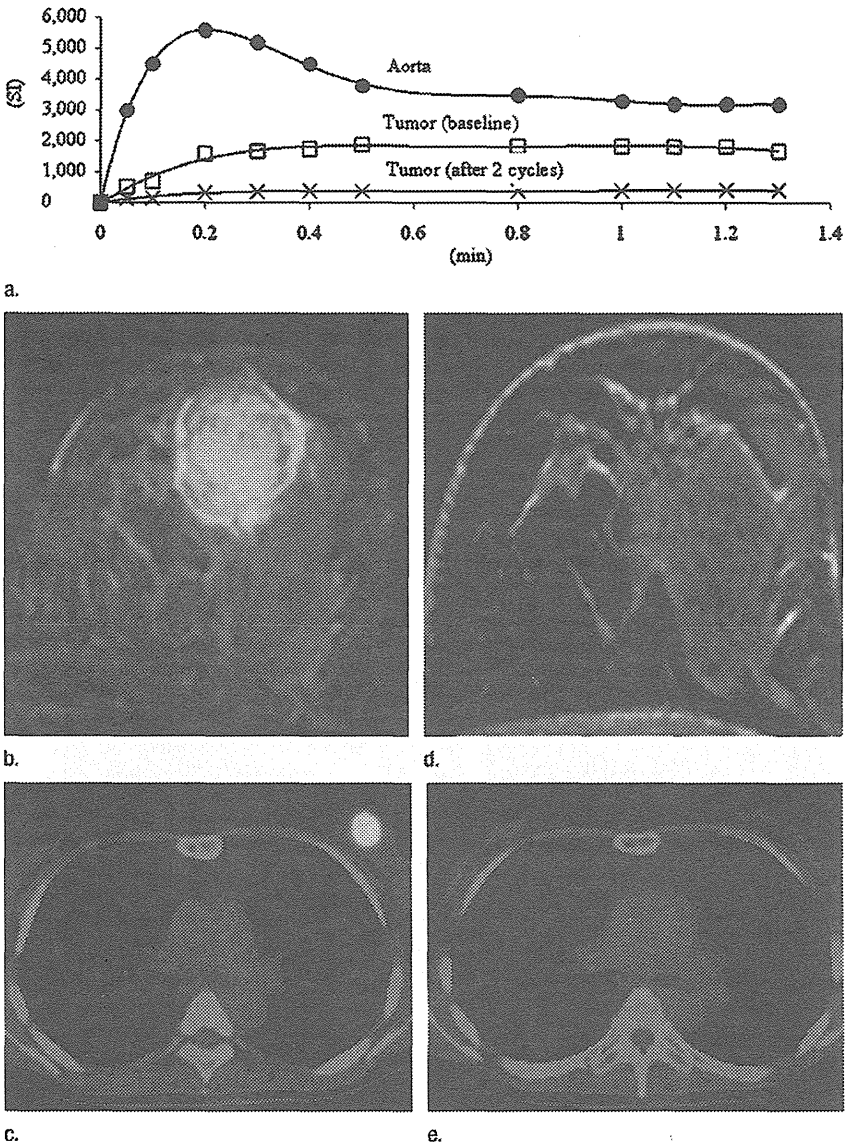

Figure 2: Changes after NAC in a 45-year-old woman with invasive ductal carcinoma of the left breast showing pCR. **(a)** Time-intensity curves. *SI* = signal intensity. Axial **(b, d)** DCE MR and **(c, e)** ^{18}F-FDG PET/CT images **(b, c)** at baseline and **(d, e)** after two cycles of NAC. Significant decrease in the mean values of all parameters from baseline was observed after two cycles of NAC: K^{trans}, from 2.7 to 0.8 1/min; κ_{ep}, from 2.0 to 0.2 1/min; AUC_{90}, from 22.1 to 8.4 mmol/L·sec; SUV_{max}, from 4.5 to 1.5 g/mL; SUL_{peak}, from 2.6 to 0.8 g/mL; and TLG, from 53.0 to 6.5 $g \cdot 10^{-3}$. The response status after two cycles of NAC was PR according to RECIST 1.1, CMR according to EORTC, and CMR according to PERCIST 1.0.

Figure 3

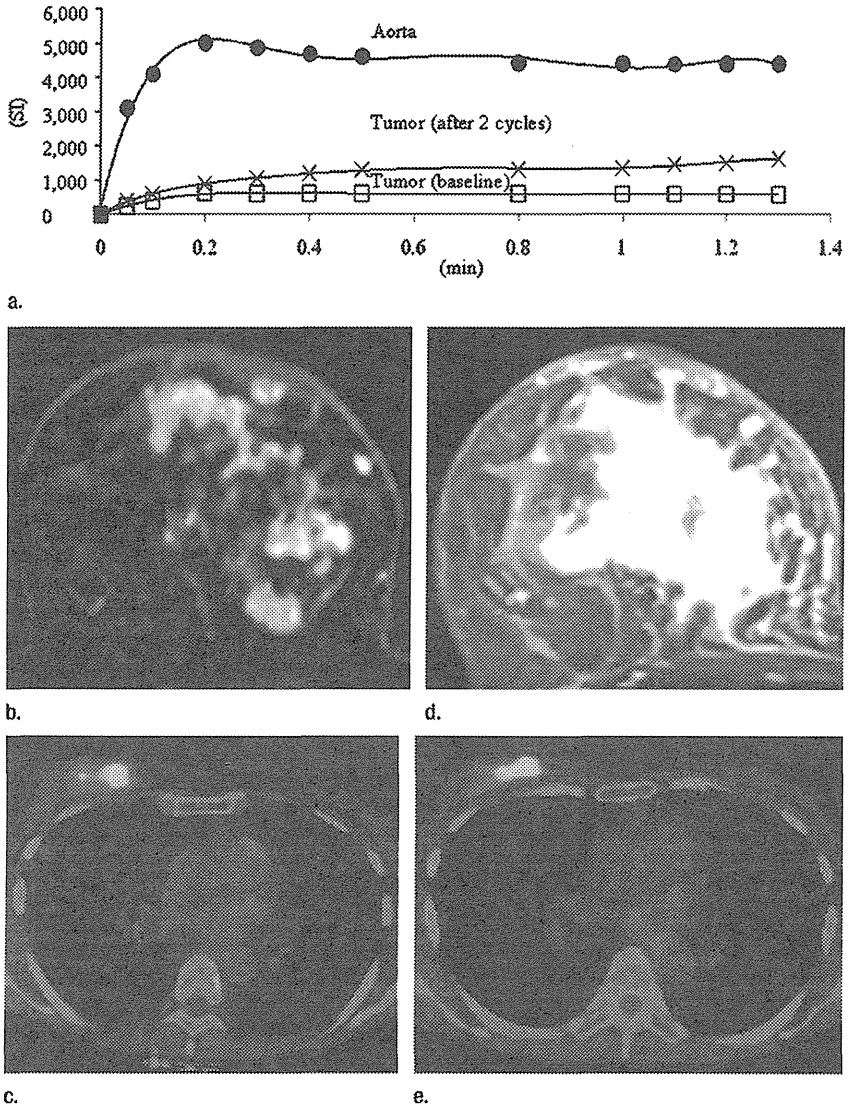

Figure 3: Changes after NAC in a 52-year-old woman with invasive ductal carcinoma of the right breast showing no pCR. **(a)** Time-intensity curves. *SI* = signal intensity. Axial **(b, d)** DCE MR and **(c, e)** ^{18}F-FDG PET/CT images **(b, c)** at baseline and **(d, e)** after two cycles of NAC. Significant increase in the mean values of all parameters from baseline was observed after two cycles of NAC: K^{trans}, from 1.6 to 4.8 1/min; κ_{ep}, from 1.1 to 3.4 1/min; AUC_{90}, from 32.5 to 68.7 mmol/L·sec; SUV_{max}, from 14.7 to 16.5 g/mL; SUL_{peak}, from 7.8 to 9.7 g/mL; and TLG, from 114.0 to 256.2 g·10^{-3}. The status after two cycles of NAC was progressive disease according to RECIST 1.1, progressive metabolic disease according to EORTC, and progressive metabolic disease according to PERCIST 1.0.

means of ^{18}F-FDG PET/CT in patients with breast cancer (5–9). However, many problems remain to be resolved, because various reference standards are set in the study protocol. In our study, we performed PET/CT studies by using the reference of pathologic response, but discrepancy between EORTC and PERCIST 1.0 criteria was found in two patients who had $\%SUV_{max}$ of 10% and 13% and $\%SUL_{peak}$ of 32% and 30%. This finding did not affect our final results, because both of these patients were assigned to the non-pCR group.

Mankoff et al (18) in a prospective analysis of 53 patients with breast cancer found that blood flow and metabolic reduction identified by direct comparison of ^{15}O water and ^{18}F-FDG PET studies were reliable predictors of progression and mortality. We observed similar findings in blood flow, microvascular permeability, and glucose metabolism identified with DCE MR imaging and ^{18}F-FDG PET/CT studies. These results suggest that it may be feasible to monitor changes in blood flow and metabolism in NAC. Since clinical trial in the NAC setting is important for testing new drugs, understanding the behavior of commonly available imaging methods will allow us to explore imaging markers. However, simultaneous PET studies with use of ^{15}O water and ^{18}F-FDG can only be performed when institutions have an on-site cyclotron. The observation that metabolic reduction after NAC was associated with the vascular parameters obtained at DCE MR imaging is reasonable. Semple et al (27) found that the vascular parameters at baseline DCE MR imaging were well correlated with the metabolic reduction in the tumor after one cycle of NAC. Their findings led to the hypothesis that metabolic reduction in the tumor might depend on the vascular supply in the baseline study. However, this finding must be viewed as inconclusive because there is as yet no evidence to suggest that the result of a two-compartment model can accurately reflect vascular supply. Furthermore, the reproducibility of the vascular parameters calculated at DCE MR imaging cannot be guaranteed, because DCE MR imaging may be affected by changes in the blood flow that may occur when acute inflammatory reaction is also present within the target lesion during NAC. In our study, the $\%SUV_{max}$ or $\%SUL_{peak}$ changed in a similar fashion to the $\%K^{trans}$, $\%\kappa_{ep}$, and $\%AUC_{90}$ during the course of NAC, especially in patients with pCR. Although the results of our study revealed that $\%SUV_{max}$, $\%\kappa_{ep}$, and $\%AUC_{90}$ were independent predictors

Table 7

Diagnostic Accuracy of $\%SUV_{max}$, $\%\kappa ep$, and $\%AUC_{90}$ to Predict pCR

Parameter	Cutoff (%)	Sensitivity (%)	Specificity (%)	PPV (%)	NPV (%)	Accuracy (%)
$\%SUV_{max}$	83.3 and 88.0	66.7 (59.0, 74.4)*†	96.4 (93.2, 99.6)	88.3 (77.1, 89.5)*†	91.5(87.0, 96.0)*†	90.1 (85.2, 95.0)*†
$\%\kappa_{ep}$	62.5 and 64.4	51.7 (43.5, 59.9)*	92.0 (87.5, 96.5)	62.5 (54.5, 70.5)*	88.1(82.8, 93.4)*	83.8 (77.7, 89.9)*
$\%AUC_{90}$	79.2 and 83.9	50.0 (42.3, 57.7)†	95.2 (91.6, 98.8)	79.2 (72.5, 85.9)†	83.9(77.9, 89.9)†	76.8 (69.9, 83.7)†

Note.—Numbers in parentheses are 95% CIs. Cutoff values of receiver operating characteristic analyses are presented as sensitivity and specificity. PPV = positive predictive value, NPV = negative predictive value.

* Significant difference between $\%SUV_{max}$ and $\%\kappa ep$ ($P < .05$).

† Significant difference between $\%SUV_{max}$ and $\%AUC_{90}$ ($P < .05$).

Table 5

Proportion of pCR and non-pCR Patients after Two Cycles of NAC according to RECIST 1.1, EORTC, and PERCIST 1.0

A: Proportion according to RECIST				
Patient Group	CR	PR	SD	PD
pCR	5 (4)	5 (4)	14 (10)	0
Non-pCR	6 (4)	48 (34)	49 (35)	15 (11)
B: Proportion according to EORTC				
Patient Group	CMR	PMR	SMD	PMD
pCR	19 (13)	5 (4)	0	0
Non-pCR	8 (6)	94 (66)	4 (3)	12 (8)
C: Proportion according to PERCIST				
Patient Group	CMR	PMR	SMD	PMD
pCR	19 (13)	5 (4)	0	0
Non-pCR	8 (6)	92 (65)	6 (4)	12 (8)

Note.—Data are numbers of patients, and numbers in parentheses are percentages. CR = complete response, PR = partial response, SD = stable disease, PD = progressive disease, CMR = complete metabolic response, PMR = partial metabolic response, SMD = stable metabolic disease, and PMD = progressive metabolic disease.

Table 6

Predictive Parameters of pCR

Parameter	Odds Ratio	95% CI	*P* Value
$\%SUV_{max}$	1.25	1.14, 1.38	<.0001
$\%\kappa_{ep}$	1.07	1.03, 1.12	.002
$\%AUC_{90}$	1.04	1.01, 1.07	.048
Combined $\%SUV_{max}$ and $\%\kappa_{ep}$	1.1	1.03, 1.36	.031

of pCR, their odds ratios were not impressive. The reason is mainly due to the fact that most patients with breast cancer cannot reach pCR after two cycles of NAC. The $\%SUV_{max}$, $\%\kappa_{ep}$, and $\%AUC_{90}$ are not sufficiently sensitive variables to be used in clinical practice, but they show high specificity to predict pCR. Furthermore, combined $\%SUV_{max}$ and $\%\kappa_{ep}$ can be also a possible predictor of pCR, but the odds ratio calculated with combined $\%SUV_{max}$ and $\%\kappa_{ep}$ was smaller than that of $\%SUV_{max}$. This may be caused by the wide range of standard deviation in $\%\kappa_{ep}$ in our study. The differences in diagnostic accuracies of $\%SUV_{max}$, $\%\kappa_{ep}$, and $\%AUC_{90}$ allow us to conclude that PET/CT is superior to DCE MR imaging in the response evaluation to NAC. However, a comparative study of both modalities is needed in the future to assess not only the response to NAC, but also the overall survival.

Wahl et al (22) recently proposed semiquantification of PET parameters, because precise response criteria are needed for comparison of studies across institutions. They use SUL, as we did in our study. The slight difference of SUV and SUL was observed in the judgment between the EORTC criteria and PERCIST 1.0 criteria. Although the judgment according to EORTC criteria and PERCIST1.0 criteria did not affect the results of our study, the results would be changed in another population or endpoint. Since most patients showed paralleled changes of $\%SUV_{max}$ and $\%SUL_{peak}$, it suggests that SUL_{peak} is a potential alternative parameter to SUV_{max}.

Our study had limitations. It must be emphasized that our study focused on patients with breast cancer who underwent NAC and that the data may not simply be extrapolated to patients with advanced-stage breast cancer. Another potential bias in this study was that the NAC regimens were diverse and the duration of follow-up was relatively short. However, these are common limitations because of the clinical need for multiple treatment regimens. Further validation in a multicenter trial with a sufficient duration of follow-up is necessary. The large number of HER-2/neu–positive patients might be recruitment bias in our study. We used

our own populations to set thresholds for data analysis, which could overestimate performance. Of importance, the cost-effectiveness of ^{18}F-FDG PET/CT and DCE MR imaging for prediction of the therapeutic effect of NAC has to be considered. Therefore, usefulness of ^{18}F-FDG PET/CT and DCE MR imaging in reducing the number of ineffective chemotherapies in patients without response must be clarified.

In conclusion, ^{18}F-FDG PET/CT and DCE MR imaging performed after two cycles of NAC allow a prediction of the pathologic response in patients with breast cancer. The $\%SUV_{max}$, $\%\kappa_{ep}$, and $\%AUC_{90}$ are not sensitive enough but are specific to be used for stratification of patients with breast cancer in clinical trials.

Disclosures of Potential Conflicts of Interest: **U.T.** No potential conflicts of interest to disclose. **M.M.** No potential conflicts of interest to disclose. **T.N.** No potential conflicts of interest to disclose. **T.T.** No potential conflicts of interest to disclose. **K.K.** No potential conflicts of interest to disclose. **T.K.** No potential conflicts of interest to disclose. **H.D.** No potential conflicts of interest to disclose. **H.A.M.** No potential conflicts of interest to disclose.

References

1. von Minckwitz G, Rezai M, Loibl S, et al. Capecitabine in addition to anthracycline- and taxane-based neoadjuvant treatment in patients with primary breast cancer: phase III GeparQuattro study. J Clin Oncol 2010;28(12):2015–2023.
2. Jeruss JS, Mittendorf EA, Tucker SL, et al. Combined use of clinical and pathologic staging variables to define outcomes for breast cancer patients treated with neoadjuvant therapy. J Clin Oncol 2008;26(2):246–252.
3. Thomas E, Holmes FA, Smith TL, et al. The use of alternate, non-cross-resistant adjuvant chemotherapy on the basis of pathologic response to a neoadjuvant doxorubicin-based regimen in women with operable breast cancer: long-term results from a prospective randomized trial. J Clin Oncol 2004;22(12):2294–2302.
4. Buzdar AU, Singletary SE, Theriault RL, et al. Prospective evaluation of paclitaxel versus combination chemotherapy with fluorouracil, doxorubicin, and cyclophosphamide as neoadjuvant therapy in patients with operable breast cancer. J Clin Oncol 1999;17(11):3412–3417.
5. Schelling M, Avril N, Nährig J, et al. Positron emission tomography using [(18)F] Fluorodeoxyglucose for monitoring primary chemotherapy in breast cancer. J Clin Oncol 2000;18(8):1689–1695.
6. Rousseau C, Devillers A, Sagan C, et al. Monitoring of early response to neoadjuvant chemotherapy in stage II and III breast cancer by [^{18}F]fluorodeoxyglucose positron emission tomography. J Clin Oncol 2006;24(34):5366–5372.
7. Berriolo-Riedinger A, Touzery C, Riedinger JM, et al. [18F]FDG-PET predicts complete pathological response of breast cancer to neoadjuvant chemotherapy. Eur J Nucl Med Mol Imaging 2007;34(12):1915–1924.
8. Duch J, Fuster D, Muñoz M, et al. 18F-FDG PET/CT for early prediction of response to neoadjuvant chemotherapy in breast cancer. Eur J Nucl Med Mol Imaging 2009;36(10):1551–1557.
9. Kumar A, Kumar R, Seenu V, et al. The role of 18F-FDG PET/CT in evaluation of early response to neoadjuvant chemotherapy in patients with locally advanced breast cancer. Eur Radiol 2009;19(6):1347–1357.
10. Choi JH, Lim HI, Lee SK, et al. The role of PET CT to evaluate the response to neoadjuvant chemotherapy in advanced breast cancer: comparison with ultrasonography and magnetic resonance imaging. J Surg Oncol 2010;102(5):392–397.
11. Emmering J, Krak NC, Van der Hoeven JJ, et al. Preoperative [18F] FDG-PET after chemotherapy in locally advanced breast cancer: prognostic value as compared with histopathology. Ann Oncol 2008;19(9):1573–1577.
12. Jung SY, Kim SK, Nam BH, et al. Prognostic Impact of [^{18}F] FDG-PET in operable breast cancer treated with neoadjuvant chemotherapy. Ann Surg Oncol 2010;17(1):247–253.
13. Pickles MD, Lowry M, Manton DJ, Gibbs P, Turnbull LW. Role of dynamic contrast enhanced MRI in monitoring early response of locally advanced breast cancer to neoadjuvant chemotherapy. Breast Cancer Res Treat 2005;91(1):1–10.
14. Padhani AR, Hayes C, Assersohn L, et al. Prediction of clinicopathologic response of breast cancer to primary chemotherapy at contrast-enhanced MR imaging: initial clinical results. Radiology 2006;239(2):361–374.
15. Ah-See ML, Makris A, Taylor NJ, et al. Early changes in functional dynamic magnetic resonance imaging predict for pathologic response to neoadjuvant chemotherapy in primary breast cancer. Clin Cancer Res 2008;14(20):6580–6589.
16. Wedam SB, Low JA, Yang SX, et al. Antiangiogenic and antitumor effects of bevacizumab in patients with inflammatory and locally advanced breast cancer. J Clin Oncol 2006;24(5):769–777.
17. Johansen R, Jensen LR, Rydland J, et al. Predicting survival and early clinical response to primary chemotherapy for patients with locally advanced breast cancer using DCE-MRI. J Magn Reson Imaging 2009;29(6):1300–1307.
18. Mankoff DA, Dunnwald LK, Gralow JR, et al. Changes in blood flow and metabolism in locally advanced breast cancer treated with neoadjuvant chemotherapy. J Nucl Med 2003;44(11):1806–1814.
19. Partridge SC, Vanantwerp RK, Doot RK, et al. Association between serial dynamic contrast-enhanced MRI and dynamic 18F-FDG PET measures in patients undergoing neoadjuvant chemotherapy for locally advanced breast cancer. J Magn Reson Imaging 2010;32(5):1124–1131.
20. Tofts PS, Brix G, Buckley DL, et al. Estimating kinetic parameters from dynamic contrast-enhanced T(1)-weighted MRI of a diffusable tracer: standardized quantities and symbols. J Magn Reson Imaging 1999;10(3):223–232.
21. Fukukita H, Senda M, Terauchi T, et al. Japanese guideline for the oncology FDG-PET/CT data acquisition protocol: synopsis of Version 1.0. Ann Nucl Med 2010;24(4):325–334.
22. Wahl RL, Jacene H, Kasamon Y, Lodge MA. From RECIST to PERCIST: Evolving Considerations for PET response criteria in solid tumors. J Nucl Med 2009;50(Suppl 1):122S–150S.
23. Boellaard R, Krak NC, Hoekstra OS, Lammertsma AA. Effects of noise, image resolution, and ROI definition on the accuracy of standard uptake values: a simulation study. J Nucl Med 2004;45(9):1519–1527.
24. Young H, Baum R, Cremerius U, et al. Measurement of clinical and subclinical tumour response using [18F]-fluorodeoxyglucose and positron emission tomography: review and 1999 EORTC recommendations. European Organization for Research and Treatment of Cancer (EORTC) PET Study Group. Eur J Cancer 1999;35(13):1773–1782.
25. Eisenhauer EA, Therasse P, Bogaerts J, et al. New response evaluation criteria in solid tumours: revised RECIST guideline (version 1.1). Eur J Cancer 2009;45(2):228–247.
26. Honkoop AH, van Diest PJ, de Jong JS, et al. Prognostic role of clinical, pathological and biological characteristics in patients with locally advanced breast cancer. Br J Cancer 1998;77(4):621–626.
27. Semple SI, Staff RT, Heys SD, et al. Baseline MRI delivery characteristics predict change in invasive ductal breast carcinoma PET metabolism as a result of primary chemotherapy administration. Ann Oncol 2006;17(9):1393–1398.

The Breast Journal

LETTER TO THE EDITOR

A Clinical Trial of Curative Surgery under Local Anesthesia for Early Breast Cancer

To the Editor:

The traditional method of surgical management of primary breast cancer has been radical mastectomy. Over the years, however, this aggressive approach has changed to a more conservative one. And now breast-conserving surgery (BCS) is the standard method. This advance was supported by the spread of breast cancer screening, the improvement of imaging methods and other developments. Moreover, the sentinel lymph node biopsy (SLNB) was developed for axillary staging (1–3). As a result, the number of cases that can avoid axillary lymph node dissection is increasing. We considered it was possible that less-invasive methods of curative management of breast cancer would be developed. Therefore, we introduced BCS with SLNB under local anesthesia (LA) for patients with early breast cancer. The aims of this article are to report our experience with BCS with SLNB performed with LA and to demonstrate the feasibility and oncological safety of this procedure.

Patients with early breast cancer (N = 23; maximum diameter, 2.0 cm, no evidence of lymph node metastases on preoperative imaging examinations) underwent BCS and SLNB under LA. The SLNB procedure was performed using a combination of radioisotope detection and blue dye or indocyanine green (ICG) fluorescence imaging. We used 15 mg pentazocine for pain reduction in the mapping material injection. Local anesthetic was administered by subcutaneous infiltration of lidocaine (1%). The skin incision was placed just on the skin marking. More local anesthetic was injected into the tissues as needed during both methods. For postoperative pain reduction, 50 mg flurbiprofen axetil was used when the skin was being closed. This method was performed with sedation using midazolam. Frozen section analysis was not used to assess the margins of resection and SLN.

The operative details of the LA group are shown in Table 1. There were no side effects of LA, and no cases needed to convert to GA. No patient suffered immediate or late surgical complications.

To assess the feasibility of using LA for this method, the results of the LA group were compared with those of the general anesthesia (GA) group (N = 36). The median age of the patients in the LA group was 60 years (range: 42–79 years), and that of the patients in the GA group was 56 years (range: 38–79 years). The median clinical tumor size was 10.0 mm for the LA group and 14.5 mm for the GA group. The procedure took a median of 77 minutes (range: 55–115 minutes) under LA and 111 minutes (range: 80–226 minutes) under GA. In six (25.0%) patients in the LA group and in eleven (30.6%) patients in the GA group, the tumor extended to 5 mm or less from the surgical margins; we defined this as a positive surgical margin. In all of the cases of both groups, SLN were identified. One patient (4.2%) in the LA group and four patients (11.1%) in the GA group had SLN that were positive for metastasis. In the GA group, frozen sections were analyzed. When the margins of resection were not free of tumor cells, we performed additional resection, and when the SLN was positive, we added complete axillary

Table 1. LA Group Cases

	n = 23
Age	60 y.o. (42–70)*
Pentazocin	15 mg (15–30)*
Midazolam	4.0 mg (0–8)*
Lidocaion	460 mg (250–700)*
Conversion to GA	0/23
Extension of hospital stay	0/23
Complications	0/23

*Median (maximum–minimum).
LA, local anesthesia; GA, general anesthesia.

Address correspondence and reprint requests to: Takahisa Hirokawa, MD, Department of Gastroenterological Surgery, Nagoya City University Graduate School of Medical Sciences, 1 Kawasumi, Mizuho-cho, Mizuho-ku, Nagoya 467-8601, Japan, or e-mail: hirokawa@med.nagoya-cu.ac.jp

DOI: 10.1111/j.1524-4741.2011.01221.x

The Breast Journal, Volume 18 Number 2, 2012 195–197

Table 2. LA Group and GA Group

	LA group $n = 23$	GA group $n = 36$
Right: left	13:10	17:19
Age	60 y.o. (42–79)*	56 y.o. (38–79)*
Tumor size	10.0 mm (2–19)*	14.5 mm (7–20)*
Operation time	77 min (55–115)*	111 min (80–226)*
Surgical cut end	6/24 (25.0%)	11/36 (30.6%)
Positive of SLN	1/24 (4.2%)	4/36 (11.1%)
Second episode of operation	1/24 (4.2%)	1/36 (2.8%)

*Median (maximum–minimum).
SLN: sentinel lymph node surgical cut end: the tumor was extended to 5 mm or less from surgical margins.
LA, local anesthesia; GA, general anesthesia.

dissection. The case in the LA group underwent complete axillary dissection on another day under general anesthesia. A case in the GA group needed additional surgery on another day under general anesthesia, because massive tumor invasion appeared in the surgical margin on the permanent specimen. Thus, one case in each group needed additional surgery on another day (Table 2).

Considering the above results, there were no differences in oncological findings between groups. No patient suffered immediate or late surgical complications. No cases of hematoma or infection were observed in the days and weeks following surgery.

Today, BCS with SLNB has become a curative surgical method for early breast cancer.

Some data regarding breast biopsy under LA have been published (4,5), and lumpectomies are often performed under LA at some centers. In addition, some reports about the feasibility of SLNB under LA have been published (6–10). Therefore, we hypothesized that curative surgical management under LA might be feasible for patients with early breast cancer. The aims of this study were to report our experience with this procedure and to evaluate the feasibility of LA and the noninferiority of LA to GA.

In this study, there were no cases that needed to convert to GA. We did not observe any acute or late complications. Moreover, none of our LA patients were uncomfortable with the procedure and all completed this method safely. Furthermore, we evaluated the points of oncology. A positive node was seen in only one case in the LA group and four cases in the GA group. Tumor invasion appeared 5 mm or less from the surgical margin in six cases in the LA group and 11 cases in the GA group in final diagnoses. There were no significant differences between the two groups. However, in the LA group, if positive nodes were seen, a second surgery under general anesthesia was necessary; on the other hand, in the GA group, such an operation could be avoided because of intraoperative frozen section examination. This is the disadvantage of management under LA, but the rate of positive nodes can be reduced by intensive preoperative imaging examinations, as was done in this study. With regard to the surgical margins, even with frozen section examination performed in the GA group, the results of the final pathological judgment were the same between groups. This result does not mean that frozen section examination is not necessary, but it does demonstrate that preoperative examination is important. In this study, the candidates we felt sure we could resect safely based on preoperative examinations were distributed to the LA group. In this way, intensive preoperative examination led to an equivalent result. Above all, there were no disadvantages oncologically in the LA group.

There are several advantages to performing curative breast cancer surgery with LA. In the LA group, because intraoperative frozen section analysis was not performed, the duration of surgery was shorter than that in the GA group. This procedure under LA leads to more efficient use of the operating room. Furthermore, it saves the pathologist time otherwise consumed by intraoperative examination. Moreover, it decreases the cost of surgery because it does not use GA, it is associated with a short hospital stay, and it does not involve intraoperative analysis of frozen sections.

Our experience indicates that curative surgery performed with LA is safe and feasible for patients with early breast cancer and may be an alternative to the standard method with GA. Above all, to undergo this method, the tumor status of the candidate must be evaluated by intensive preoperative examination.

Takahisa Hirokawa, MD
Takayuki Kinoshita, MD
Tomoya Nagao, MD
Takashi Hojo, MD
Department of Surgery and Division of Breast Cancer,
National Cancer Center Hospital, Tokyo, Japan

REFERENCES

1. Schwartz GF, Giuliano AE, Veronesi U, *et al.* Proceedings of the consensus conference on the role of sentinel lymph node biopsy in carcinoma of the breast April 19 to 22, 2001, Philadelphia, Pennsylvania. *Hum Pathol* 2002;33:579–89.

2. Veronesi U, Paganelli G, Viale G, *et al.* A randomized comparison of sentinel-node biopsy with routine axillary dissection in breast cancer. *N Engl J Med* 2003;349:546–53.

3. Veronesi U, Paganelli G, Viale G, *et al.* Sentinel-lymph-node biopsy as a staging procedure in breast cancer: update of a randomised controlled study. *Lancet Oncol* 2006;7:983–90.

4. Lou MA, Mandal AK, Alexander JL. The pros and cons of outpatient breast biopsy. *Arch Surg* 1976;111:668–70.

5. Baker RR. Out-patient breast biopsies. *Ann Surg* 1977;185:543–7.

6. Fenaroli P, Tondini C, Motta T, Virotta G, Personeni A. Axillary sentinel node biopsy under local anaesthesia in early breast cancer. *Ann Oncol* 2000;11:1617–8.

7. Luini A, Gatti G, Frasson A, *et al.* Sentinel lymph node biopsy performed with local anesthesia in patients with early-stage breast carcinoma. *Arch Surg* 2002;137:1157–60.

8. Smidt ML, Janssen CM, Barendregt WB, Wobbes T, Strobbe LJ. Sentinel lymph node biopsy performed under local anesthesia is feasible. *Am J Surg* 2004;187:684–7.

9. Luini A, Caldarella P, Gatti G, *et al.* The sentinel node biopsy under local anesthesia in breast cancer: advantages and problems, how the technique influenced the activity of a breast surgery department; update from the European Institute of Oncology with more than 1000 cases. *Breast* 2007;16:527–32.

10. Van Berio CL, Hess DA, Nijhuis PA, Leys E, Gerritsen HA, Schapers RF. Ambulatory sentinel node biopsy under local anaesthesia for patients with early breast cancer. *Eur J Surg Oncol* 2003;29: 383–5.

Cancer Letters 322 (2012) 204–212

Contents lists available at SciVerse ScienceDirect

Cancer Letters

journal homepage: www.elsevier.com/locate/canlet

Development of a novel approach, the epigenome-based outlier approach, to identify tumor-suppressor genes silenced by aberrant DNA methylation

Mizuho Kikuyama [a,b], Hideyuki Takeshima [a], Takayuki Kinoshita [c], Eriko Okochi-Takada [a], Mika Wakabayashi [a], Sadako Akashi-Tanaka [c], Toshihisa Ogawa [b], Yasuyuki Seto [b], Toshikazu Ushijima [a,*]

[a] Division of Epigenomics, National Cancer Center Research Institute, 5-1-1 Tsukiji, Chuo-ku, 104-0045 Tokyo, Japan
[b] Department of Metabolic Care and Endocrine Surgery, Graduate School of Medicine, The University of Tokyo, 7-3-1 Hongo, Bunkyo-ku, 113-8655 Tokyo, Japan
[c] Breast Surgery Division, National Cancer Center Hospital, 5-1-1 Tsukiji, Chuo-ku, 104-0045 Tokyo, Japan

ARTICLE INFO

Article history:
Received 4 January 2012
Received in revised form 10 March 2012
Accepted 12 March 2012

Keywords:
Epigenetics
Aberrant DNA methylation
Tumor-suppressor gene

ABSTRACT

Identification of tumor-suppressor genes (TSGs) silenced by aberrant methylation of promoter CpG islands (CGIs) is important, but hampered by a large number of genes methylated as passengers of carcinogenesis. To overcome this issue, we here took advantage of the fact that the vast majority of genes methylated in cancers lack, in normal cells, RNA polymerase II (Pol II) and have trimethylation of histone H3 lysine 27 (H3K27me3) in their promoter CGIs. First, we demonstrated that three of six known TSGs in breast cancer and two of three in colon cancer had Pol II and lacked H3K27me3 in normal cells, being outliers to the general rule. *BRCA1*, *HOXA5*, *MLH1*, and *RASSF1A* had high Pol II, but were expressed only at low levels in normal cells, and were unlikely to be identified as outliers by their expression statuses in normal cells. Then, using epigenome statuses (Pol II binding and H3K27me3) in normal cells, we made a genome-wide search for outliers in breast cancers, and identified 14 outlier promoter CGIs. Among these, *DZIP1*, *FBN2*, *HOXA5*, and *HOXC9* were confirmed to be methylated in primary breast cancer samples. Knockdown of *DZIP1* in breast cancer cell lines led to increases of their growth, suggesting it to be a novel TSG. The outliers based on their epigenome statuses contained unique TSGs, including *DZIP1*, compared with those identified by the expression microarray data. These results showed that the epigenome-based outlier approach is capable of identifying a different set of TSGs, compared to the expression-based outlier approach.

1. Introduction

Aberrant DNA methylation of promoter CpG islands (CGIs), especially that of nucleosome-free regions (NFRs), causes silencing of their downstream genes [1], and is known as an alternative mechanism to point mutations and chromosomal deletion for inactivation of tumor-suppressor genes (TSGs) [2–6]. Now, TSGs involved in various biological pathways such as cell proliferation, cell adhesion, and DNA repair are known to be silenced by aberrant DNA methylation in human cancers [7,8]. To identify novel TSGs silenced by aberrant DNA methylation, two major approaches for genome-wide screening have been reported, namely (1) genome-wide screening of methylated genes and (2) screening of genes whose expression is induced by a DNA demethylating agent (chemical genomic screening) [9–13].

A genome-wide screening of methylated genes usually isolates several hundreds to one thousand genes whose promoter CGIs are methylated in cancers [12,14]. Unfortunately, most of these genes are not expressed or expressed at only low levels in normal cells [14]. Since genes with low transcription tend to be methylated [15], most of the genes identified by genome-wide screening of methylated genes are considered to be methylated as a consequence of carcinogenesis. In chemical genomic screening, cell lines are treated with a DNA demethylating agent, 5-aza-2′-deoxycytidine (5-aza-dC), and genes whose expression is induced are screened by expression microarray analysis. However, since 5-aza-dC forms DNA adducts [16] and induces double-strand breaks [17], treatment with 5-aza-dC leads to up-regulation of not only methylation-silenced genes but also numerous genes involved in responses to DNA damage, including p53-activated genes [18–21].

It was recently shown that the vast majority of genes aberrantly methylated in cancers have specific epigenetic statuses in normal cells, namely the lack of RNA polymerase II (Pol II) and the presence of trimethylation of histone H3 lysine 27 (H3K27me3) [14,22]. H3K27me3 is known to be most influential on the susceptibility of genes to become methylated among various histone

Abbreviations: CGIs, CpG islands; ChIP, chromatin immunoprecipitation; FHC, normal fetal human colon epithelial cell line; HMECs, normal human mammary epithelial cells; H3K27me3, trimethylation of histone H3 lysine 27; NFR, nucleosome-free region; Pol II, RNA polymerase II; TSG, tumor-suppressor gene.

* Corresponding author. Fax: +81 3 5565 1753.
E-mail address: tushijim@ncc.go.jp (T. Ushijima).

0304-3835/$ - see front matter © 2012 Elsevier Ireland Ltd. All rights reserved.
http://dx.doi.org/10.1016/j.canlet.2012.03.016

modifications [14]. At the same time, approximately 5% of the genes methylated in cancers do not follow the general rule [14], constituting a group of "outliers". Since a TSG is functioning in normal cells, it is expected to have Pol II in normal cells and belong to the outliers. Even if silencing of a TSG is a very rare event due to the Pol II binding, a cell with its silencing will become dominant due to the resultant growth advantage, and the TSG appears as if it is susceptible to methylation. Indeed, by searching outliers with high expression in normal cells, TSGs have been successfully identified [11,23,24]. However, some TSGs, including *CDKN1A*, are known to have no or low expression in normal cells and are activated by extracellular stimuli [25,26].

In this study, we aimed to show that a significant fraction of known TSGs silenced by aberrant DNA methylation are outliers. Then, we will show that a different set of TSGs could be identified by searching for outliers with high Pol II and without H3K27me3 (epigenome-based outlier approach), compared to those identified by searching for outliers with high expression (expression-based outlier approach).

2. Materials and methods

2.1. Cell lines and primary breast cancer samples

Human breast cancer cell lines (BT-20, BT-474, HCC38, HCC1428, HCC1937, Hs 578T, MCF7, MDA-MB-231, MDA-MB-436, MDA-MB-468, SK-BR-3, T-47D, and ZR-75-1), normal fetal human colon epithelial cell line (FHC), and 293TN cell line were purchased from the American Type Culture Collection (Rockville, MD). Normal human mammary epithelial cells (HMECs) were purchased from Cambrex (East Rutherford, NL). Forty primary breast cancer samples were obtained from patients who underwent mastectomy or breast conserving surgery with informed consent. Resected primary samples were frozen and stored at −80 °C until the extraction of genomic DNA. The analysis was approved by the Institutional Review Boards.

2.2. Chromatin immunoprecipitation (ChIP)

Eight μg of chromatin extracted from HMECs was incubated with 0.7 μg of antibodies against Pol II (ab5095; Abcam, Cambridge, UK) or H3K27me3 (07-449; Millipore, Billerica, MA) overnight at 4 °C. Then the immunocomplex was collected with Dynabeads Protein A (Invitrogen Dynal AS, Oslo, Norway). Recovered DNA was dissolved in 33 μl of 1 × TE (10 mM Tris-HCl and 1 mM EDTA) [14], and one μl of DNA was used for ChIP-quantitative PCR (ChIP-qPCR) using primer sets listed in Supplementary Table 1. The specificity of the ChIP assay was assessed by using primers for control regions whose histone modification statuses were already known [14] (Supplementary Fig. 1).

2.3. Analyses of microarray data

DNA methylation data of 9838 promoter CGIs in HMECs, BT-474, MCF7, MDA-MB-231, MDA-MB-468, and ZR-75-1 were obtained from our previous study using methylated DNA immunoprecipitation (MeDIP)-CGI microarray analysis [27]. Pol II binding and H3K27me3 data of 9838 promoter CGIs in HMECs were obtained from our previous study using ChIP-CGI microarray analysis [14]. Pol II binding and H3K27me3 levels of each CGI were evaluated using the average of the signal ratio [Cy5 signal (bound)/Cy3 signal (input)] of the probes within a NFR. CGIs with a mean signal ratio larger than that at the 80th percentile of the total probes were considered as CGIs with high Pol II binding or H3K27me3, and those with an average signal ratio smaller than that at the 20th percentile of the total probes were considered as CGIs with low Pol II binding or H3K27me3. Other CGIs were considered as genes with intermediate Pol II binding or H3K27me3 levels. Gene expression data in HMECs were obtained from our previous study using the GeneChip Human Genome U133 Plus 2.0 microarray (Affymetrix, Santa Clara, CA), and genes were classified into those with high, moderate, and low expression levels, as described previously [14].

2.4. Quantitative methylation-specific PCR (qMSP)

Genomic DNA was digested with *Bam*HI, and one μg of digested DNA was used for bisulfite modification [28]. qMSP was performed using primer sets specific to methylated target loci and to the *Alu* repeat sequence (Supplementary Table 2). Modified DNA was dissolved in 40 μl of 1 × TE, and one μl was used for qMSP. The number of DNA molecules in a sample was obtained by comparing its amplification curve with those of standard samples with known numbers of DNA molecules. DNA methylation levels were calculated as the percentage of the methylation reference (PMR) = [(number of molecules methylated at a target CGI in a sample)/(number of *Alu* repeat sequences in the sample)]/[(number of molecules methylated at the target CGI in a fully methylated DNA)/(number of *Alu* repeat sequences in the fully methylated DNA)] × 100 [29,30]. Genomic DNA treated with *SssI* methylase (New England Biolabs, Beverly, MA) was used as a fully methylated DNA. Since the copy number of the target CGI was normalized to the copy number of the *Alu* repeat sequence, PMR could reach more than 100% when the locus containing the target CGI had an increased copy number.

2.5. Quantitative reverse transcription-PCR (qRT-PCR)

Total RNA was isolated using ISOGEN (Nippon Gene, Tokyo, Japan). cDNA was synthesized from one μg of total RNA using SuperScript III reverse transcriptase and an oligo $(dT)_{12-18}$ primer (Life Technologies, Carlsbad, CA). qRT-PCR was performed using primer sets listed in Supplementary Table 3, as described previously [31]. The number of cDNA molecules in a sample was obtained by comparing its amplification curve with those of standard samples with known numbers of cDNA molecules, and the number of target cDNA molecules was normalized to those of human *GAPDH* cDNA molecules.

2.6. 5-Aza-dC and trichostatin A (TSA) treatment

T-47D cells were seeded on day 0, and exposed to a designated dose of freshly prepared 5-aza-dC (SIGMA-ALDRICH, St. Louis, MO) for 24 h on days 1 and 3, and treated with TSA (SIGMA-ALDRICH) on day 4. The cells were harvested on day 5, and total RNA was extracted.

2.7. Knockdown of DZIP1 and cell growth assay

DZIP1 was knocked down by two different short hairpin RNAs (shRNA1 and shRNA2; Supplementary Table 4) designed by using siDirect version 2.0 [32], and shRNA for firefly luciferase was used as the control. The sense and antisense oligonucleotides containing each shRNA sequence were annealed, and then ligated into *Bam*HI/*Eco*RI sites of pGreenPuro™ shRNA Cloning and Expression Lentivector (System Biosciences, Mountain View, CA). The shRNA expression construct was co-transfected with pPACK Packaging Plasmid Mix (System Biosciences) into 293TN cells using Lipofectamine™ with Plus™ Reagent (Life Technologies). Medium containing pseudovirus was collected 48 h after transfection, and stored at −80 °C until use. HCC1937 and MDA-MB-436 cells were infected with pseudovirus according to the manufacturer's protocol.

Cell growth was analyzed by seeding cells at a density of 5×10^4 cells/6 cm plate on day 0, and counting the cell numbers on days 1, 2, 3, 4, 5, and 8 using TC™ Automated Cell Counter (Bio-Rad Laboratories, Hercules, CA).

3. Results

3.1. Confirmation of known TSGs as outliers

To confirm that TSGs are outliers to the general rule of genes methylated in cancer cells, we first analyzed six known TSGs silenced in breast cancer by aberrant DNA methylation, *BRCA1*, *CDKN2A* (*p16*), *HOXA5*, *MASPIN*, *RASSF1A*, and *RBP1* [33–38]. The Pol II binding and H3K27me3 levels of these six genes were analyzed in HMECs (Fig. 1A). Among the six TSGs, *BRCA1*, *HOXA5*, and *MASPIN* had high Pol II binding and almost undetectable levels of H3K27me3 in the HMECs, demonstrating that these genes are outliers. In contrast, *RASSF1A* had low Pol II binding and high H3K27me3 levels, showing that *RASSF1A* was methylated according to the rule. *CDKN2A* and *RBP1* had intermediate levels of Pol II binding and H3K27me3. We also analyzed expression levels of the six TSGs in normal cells. Among the three outliers, *MASPIN* was expressed at high levels (active Pol II), and *BRCA1* and *HOXA5* were expressed at low levels (stalled Pol II) (Fig. 1C). In the case of three TSGs known to be methylation-silenced in colon cancer, *MLH1* and *RASSF1A* [7] had high levels of Pol II binding and low expression levels (stalled Pol II) (Fig. 1B and D). These results indicated that a significant fraction of TSGs are "outliers" to the general rule of genes methylated in cancer cells, and that the outliers could be classified into those with active Pol II and with stalled Pol II.

3.2. Screening of outliers in breast cancer based on their epigenome statuses

Confirming that three of six known TSGs in breast cancer and two of three known TSGs in colon cancer are outliers, we pro-

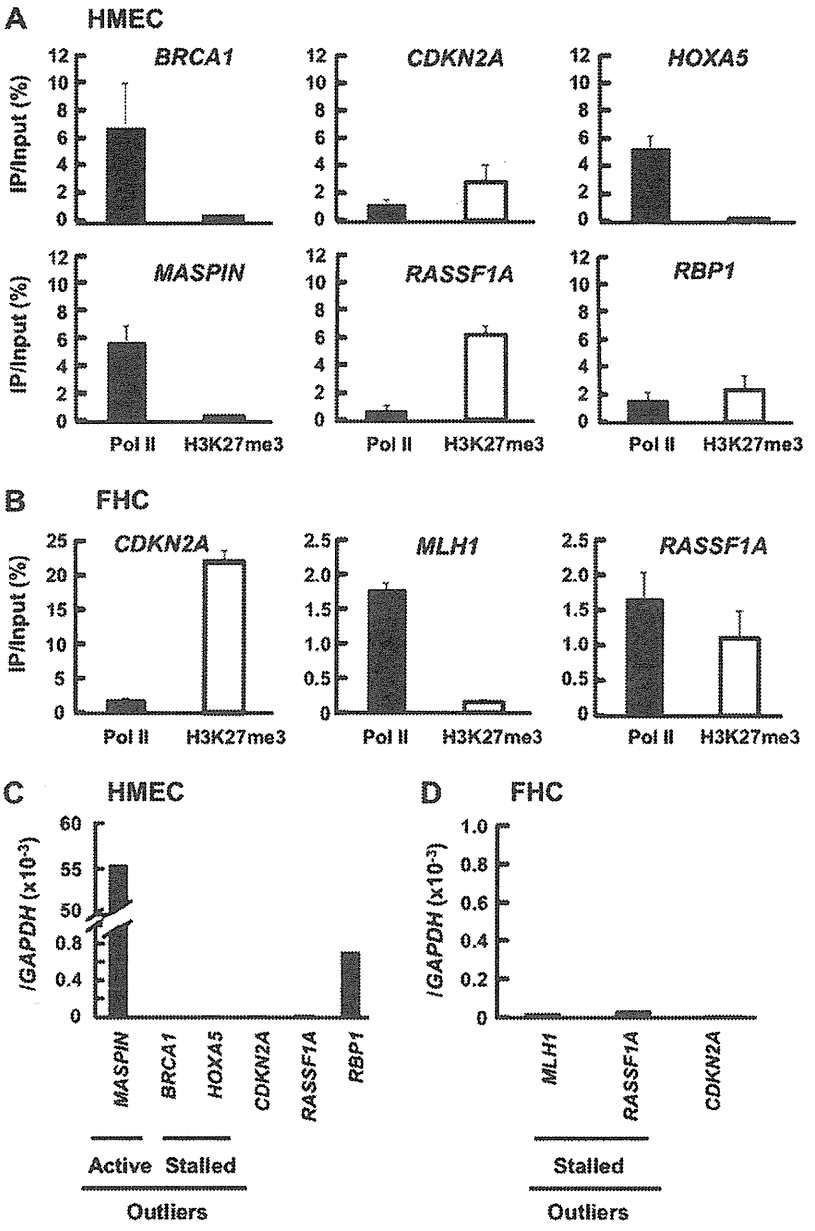

Fig. 1. Confirmation of known TSGs as outliers to the general rule. (A) Pol II binding and H3K27me3 levels in HMECs of the six TSGs in breast cancer analyzed by ChIP-qPCR. Three of the six TSGs showed relatively high Pol II binding levels and low H3K27me3 levels in the HMECs, showing that they are outliers to the general rule. The mean ± SE values of three independent experiments are shown. (B) Pol II binding and H3K27me3 levels in FHC of the three TSGs in colon cancer analyzed by ChIP-qPCR. Two of the three TSGs showed high Pol II binding and low H3K27me3 levels, being outliers. (C) and (D) Expression levels of the known TSGs in normal cells. Expression levels of TSGs in HMECs (C) and FHC (D) were analyzed by qRT-PCR. Among the five outliers in breast and colon cancers, only *MASPIN* was expressed at high levels in HMECs, and the other four outliers were expressed at low levels. Active; active Pol II, Stalled; stalled Pol II.

ceeded to identify novel TSGs in breast cancer by making a genome-wide search for outliers. Based on DNA methylation statuses of two different lots of normal breast epithelial cells (HMECs) and five breast cancer cell lines obtained by MeDIP-CGI microarray analyses, we previously identified 280 promoter CGIs unmethylated in both lots of the HMECs and methylated in two or more of the breast cancer cell lines as methylation-susceptible promoter CGIs in breast cancer [27]. To identify outliers based on the epigenome statuses, Pol II binding and H3K27me3 statuses in the HMECs [14] were utilized. Among the 280 promoter CGIs susceptible to methylation induction during breast carcinogenesis, 37 CGIs had high Pol II binding (Fig. 2A), and 14 of the 37 CGIs had low H3K27me3 levels in the HMECs (Fig. 2B). Since two promoter CGIs were shared by two genes, respectively, 16 genes downstream of these 14 promoter CGIs were considered as outliers in breast cancers (Table 1).

3.3. DNA methylation of outlier promoter CGIs in primary breast cancer samples

DNA methylation levels were quantified by qMSP for 13 of the 14 promoter CGIs (except for a CGI upstream of two core histone genes) in 13 breast cancer cell lines, including the five breast cancer cell lines used for identification of methylation-susceptible promoter CGIs, and HMECs (Fig. 3A and Supplementary Fig. 2). All the 13 outlier promoter CGIs showed low methylation in the HMECs, and five (*DZIP1*, *FBN2*, *HOXA5*, *HOXC9*, and *OSBPL3*) of them showed

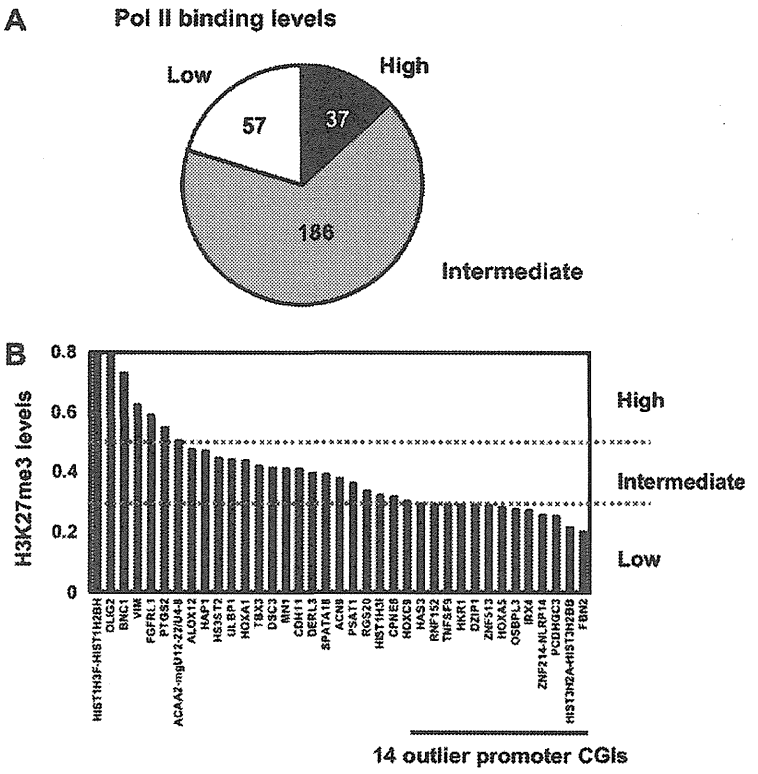

Fig. 2. Genome-wide screening of outliers based on the epigenome. (A) Pol II binding levels of the 280 methylation-susceptible promoter CGIs in the HMECs. Thirty-seven CGIs (13% of susceptible CGIs) showed high Pol II binding levels in the HMECs. (B) H3K27me3 levels of the 37 CGIs with high Pol II binding in the HMECs. Fourteen promoter CGIs with high Pol II binding levels showed low H3K27me3 levels in the HMECs, being outliers.

Table 1
List of outlier promoter CGIs in breast cancer.

	Gene symbol	Gene name	Chr	DNA methylation						
				Normal		Cancer				
				HMEC#1	HMEC#2	BT-474	MCF7	MDA-MB-231	MDA-MB-468	ZR-75-1
1	*DZIP1*	DAZ interacting protein 1	13	UM	UM	UM	HM	UM	HM	MM
2	*FBN2*[a]	Fibrillin 2	5	UM	UM	UM	MM	HM	HM	UM
3	*HAS3*	Hyaluronan synthase 3	16	UM	UM	MM	HM	MM	MM	HM
4	*HIST3H2A-HIST3H2BB*[b]	Histone cluster 3, H2a/histone cluster 3, H2bb	1	UM	UM	UM	UM	HM	HM	UM
5	*HKR1*	GLI-Kruppel zinc family member	19	UM	UM	UM	UM	HM	UM	HM
6	*HOXA5*[a]	Homeobox A5	7	UM	UM	UM	UM	HM	HM	HM
7	*HOXC9*	Homeobox C9	12	UM	UM	UM	UM	HM	HM	UM
8	*IRX4*	Iroquois homeobox 4	5	UM	UM	UM	UM	HM	HM	UM
9	*OSBPL3*	Oxysterol binding protein-like 3	7	UM	UM	HM	HM	UM	UM	UM
10	*PCDHGC3*	Protocadherin gamma subfamily C, 3	5	UM	UM	UM	UM	HM	HM	UM
11	*RNF152*	Ring finger protein 152	18	UM	UM	UM	UM	HM	HM	UM
12	*TNFSF9*	Tumor necrosis factor (ligand) superfamily, member 9	19	UM	UM	HM	UM	UM	HM	UM
13	*ZNF214-NLRP14*[b]	Zinc finger protein 214/NLR family, pyrin domain containing 14	11	UM	UM	UM	HM	UM	HM	UM
14	*ZNF513*	Zinc finger protein 513	2	UM	UM	UM	HM	HM	UM	HM

UM, unmethylated; MM, moderately methylated; HM, highly methylated; chr, chromosome number.
[a] Known tumor-suppressor gene.
[b] Promoter CGIs shared by two genes.

high methylation levels (PMR higher than 100%) in at least one cancer cell line (Fig. 3A).

Then, using 40 primary breast cancer samples, the methylation levels of these five outlier promoter CGIs were analyzed. Methylation of *DZIP1*, *FBN2*, *HOXA5*, and *HOXC9* was present in primary breast cancer samples, while that of *OSBPL3* was not observed (Fig. 3B). These results indicated that *DZIP1*, *FBN2*, *HOXA5*, and *HOXC9* are outliers methylated not only in cell lines but also in primary breast cancers. Among the four outliers, *HOXA5* and *FBN2* were known as TSGs silenced by aberrant DNA methylation in